

PHASE TRANSFORMATION AND MAGNETIC PROPERTIES OF
MULTICOMPONENT HEUSLER TYPE ALLOYS

A THESIS SUBMITTED TO
THE GRADUATE SCHOOL OF NATURAL AND APPLIED SCIENCES
OF
MIDDLE EAST TECHNICAL UNIVERSITY

BY

MİNE KALKANCI

IN PARTIAL FULFILLMENT OF THE REQUIREMENTS
FOR
THE DEGREE OF MASTER OF SCIENCE
IN
METALLURGICAL AND MATERIALS ENGINEERING

SEPTEMBER 2011

Approval of the thesis:

**PHASE TRANSFORMATION AND MAGNETIC PROPERTIES OF
MULTICOMPONENT HEUSLER TYPE ALLOYS**

Submitted by **MİNE KALKANCI** in partial fulfillment of the requirements for the degree of **Master of Science in Metallurgical and Materials Engineering Department, Middle East Technical University** by,

Prof. Dr. Canan Özgen _____
Dean, Graduate School of **Natural and Applied Sciences**

Prof. Dr. Tayfur Öztürk _____
Head of Department, **Metallurgical and Materials Engineering**

Prof. Dr. M. Vedat Akdeniz _____
Supervisor, **Metallurgical and Materials Engineering Dept., METU**

Prof. Dr. Amdulla O. Mekhrabov _____
Co-Supervisor, **Metallurgical and Materials Engineering Dept., METU**

Examining Committee Members:

Assoc. Prof. Dr. Caner Durucan _____
Metallurgical and Materials Engineering Dept., METU

Prof. Dr. M. Vedat Akdeniz _____
Metallurgical and Materials Engineering Dept., METU

Prof. Dr. Amdulla O. Mekhrabov _____
Metallurgical and Materials Engineering Dept., METU

Assist. Prof. Dr. Y. Eren Kalay _____
Metallurgical and Materials Engineering Dept., METU

Assist. Prof. Dr. Ziya Esen _____
Materials Science and Engineering Dept., ÇANKAYA UNI.

Date: 15 September 2011

I hereby declare that all information in this document has been obtained and presented accordance with the academic rules and ethical conduct. I also declare that, as required by these rules and conduct, I have fully cited and referenced all material and results that are not original to this work.

Name, Last name: Mine Kalkanci

Signature :

ABSTRACT

PHASE TRANSFORMATION AND MAGNETIC PROPERTIES OF MULTICOMPONENT HEUSLER TYPE ALLOYS

Kalkanci, Mine

M.Sc. Department of Metallurgical and Materials Engineering

Supervisor: Prof. Dr. M. Vedat Akdeniz

Co-Supervisor: Prof. Dr. Amdulla O. Mekhrabov

September 2011, 77 pages

Many Co-based Heusler alloys with the stoichiometric composition X_2YZ are ideal candidates for the spintronics applications. So, they have been extensively studied theoretically and experimentally. The aim of this work was to investigate the effect heat treatment on phase stability and magnetic properties for quaternary $Co_2FeSi_{1-x}Ga_x$ Heusler alloys with varying Si concentration. The $Co_2FeSi_{1-x}Ga_x$ alloy samples were prepared by conventional arc melting technique. The structure of $Co_2FeSi_{1-x}Ga_x$ bulk alloys were examined by powder x-ray diffraction and differential scanning calorimetry. It was confirmed that $Co_2FeSi_{1-x}Ga_x$ alloys display the $L2_1$ type structure for all x compositions based on the annealing temperature. The magnetic ordering transition temperature, T_c , was measured by differential scanning calorimetry. It was found that the order-disorder phase transition temperature from the $L2_1$ to the B2 structure, $T_{L2_1/B2}$, decreases while the Curie temperature, T_c , increases with increasing x ; however, the value of these temperatures were not influenced by changing heat treatment process. The magnetic properties of $Co_2FeSi_{1-x}Ga_x$ alloy were investigated by using vibrating sample magnetometer. Higher saturation value was obtained at the $L2_1$ phase than the value obtained at the

B2 phase. It was concluded that the $\text{Co}_2\text{FeSi}_{0.2}\text{Ga}_{0.8}$ alloy was chosen optimum composition for spintronics applications because of its highest Curie temperature and phase stability of $L2_1$.

Keywords: Heusler Alloys, Order-Disorder Phenomena, Curie Temperature, Magnetic Properties, Heat Treatment.

ÖZ

ÇOK BİLEŞENLİ HEUSLER TİPİ ALAŞIMLARIN FAZ DÖNÜŞÜMLERİ VE MANYETİK ÖZELLİKLERİ

Kalkanci, Mine

Yüksek Lisans, Metalurji ve Malzeme Mühendisliği Bölümü

Tez Yöneticisi: Prof. Dr. M. Vedat Akdeniz

Ortak Tez Yöneticisi: Prof. Dr. Amdulla O. Mekhrabov

Eylül 2011, 77 sayfa

Stokiometrik bileşimi X_2YZ şeklinde olan birçok Co-bazlı Heusler alaşımları spintronik uygulamalar için ideal adaylardır. Bu nedenle, bunlar teorik ve deneysel olarak yaygın şekilde çalışılmıştır. Bu çalışmanın amacı, farklı Si konsantrasyonuna sahip dördü Heusler alaşımları ($Co_2FeSi_{1-x}Ga_x$) için tavlama sıcaklığının, faz kararlılığı ve manyetik özellikleri üzerindeki etkisini araştırmaktır. $Co_2FeSi_{1-x}Ga_x$ alaşım numuneleri bilinen ark eritme tekniği ile hazırlanmıştır. $Co_2FeSi_{1-x}Ga_x$ yığını toz x-ışını kırınımı ve diferansiyel taramalı kalorimetre ile incelenmiştir. $Co_2FeSi_{1-x}Ga_x$ alaşımının, tavlama sıcaklığına bağlı olarak bütün x değerleri için $L2_1$ tip yapı gösterdiği görülmüştür. Yapısal faz geçiş sıcaklığı, Ga konsantrasyonunun artmasıyla azalmaktadır. Curie sıcaklığı diferansiyel taramalı kalorimetre ile ölçülmüştür. Curie sıcaklığının (T_C) artan x değeriyle artarken, $L2_1$ 'den B_2 yapısına geçişteki düzenlilik-düzensizlik faz dönüşüm sıcaklığının (T_{L2_1}) azaldığı; ancak bu sıcaklık değerlerinin tavlama sıcaklığındaki değişimden etkilenmediği bulunmuştur. $Co_2FeSi_{1-x}Ga_x$ alaşımının manyetik özellikleri titreşim manyetometresi kullanılarak incelenmiştir. $L2_1$ fazında, B_2 fazında elde edilenden daha yüksek doygunluk değeri elde edilmiştir. $Co_2FeSi_{0.2}Ga_{0.8}$ alaşımının, en yüksek Curie sıcaklığı ve $L2_1$ faz

kararlılığına sahip olmasından dolayı spintronik uygulamalar için en uygun kompozisyon olduğu sonucuna varılmıştır.

Anahtar Sözcükler: Heusler Alaşımları, Düzen – Düzensizlik Kavramı, Curie Sıcaklığı, Manyetik Özellikler, Isıl İşlem.

To my Family...

ACKNOWLEDGEMENTS

I would like to express my special thanks to my supervisors Prof. Dr. M. Vedat Akdeniz and Prof. Dr. Amdulla O. Mekhrabov for their continuous guidance, support, motivation and encouragement during this study. I sincerely appreciate the time and effort they have spent to improve my experience during my thesis.

I deeply thank to special lab mates Mehmet Yıldırım, Muratahan Aykol, Nagehan Duman, Tufan Güngören for their helpful discussions and support during my experiments. I also would like to thank my friends Özlem Çağlar, Şafak Halıcı, Aysel Kızıltay, Eylem Yalçınkaya, Tuğba Endoğan, Ayfer Özdemir, Seher Karabıçak, Özlem Oktay, Özlem Altıntaş Yıldırım and Nihat Ali Işıtman for their support and friendship during graduate years.

Finally, I would like to thank to my mother Aysel Kalkanci, my father Mecit Kalkanci, my sister Müge Kalkanci, my aunts Şenay Erdenir and Hatice Kundakçioğlu, for their love and patience they have shown throughout my life.

TABLE OF CONTENT

ABSTRACT	iv
ÖZ	vi
ACKNOWLEDGEMENTS	ix
TABLE OF CONTENTS	x
LIST OF TABLES	xiii
LIST OF FIGURES.....	xv
LIST OF SYMBOLS	xx
CHAPTERS	
1. INTRODUCTION	1
2. HEUSLER ALLOYS	3
2.1 THE FULL HEUSLER ($L2_1$ TYPE) STRUCTURE	3
2.2 ORDER-DISORDER STRUCTURAL TRANSFORMATION.....	5
2.2.1 STRUCTURE DETERMINATION.....	7
2.3 MAGNETISM IN HEUSLER ALLOYS	9
2.3.1 FERROMAGNETS.....	10
2.3.1.1 HALF-METALIC FERROMAGNETIC.....	13

3. EXPERIMENTAL PROCEDURE.....	16
3.1 SAMPLE PREPARATION	16
3.2 SAMPLE CHARACTERIZATION	17
4. RESULTS AND DISCUSSIONS	20
4.1 STRUCTURAL AND MAGNETIC PROPERTIES AND PHASE TRANSFORMATION TEMPERATURES OF THE AS-CAST $\text{Co}_2\text{FeSi}_{1-x}\text{Ga}_x$ ALLOY SYSTEM	20
4.1.1 EFFECTS OF COMPOSITION ON STRUCTURAL PROPERTIES OF THE AS-CAST $\text{Co}_2\text{FeSi}_{1-x}\text{Ga}_x$ ALLOY SYSTEM.....	21
4.1.2 EFFECTS OF COMPOSITION ON THE PHASE TRANSFORMATION TEMPERATURES OF THE AS-CAST $\text{Co}_2\text{FeSi}_{1-x}$ Ga_x ALLOY SYSTEM.....	22
4.1.3 EFFECTS OF COMPOSITION ON THE MAGNETIC PROPERTIES OF THE AS-CAST $\text{Co}_2\text{FeSi}_{1-x}\text{Ga}_x$ ALLOY SYSTEM.....	23
4.2 EFFECT OF HEAT TREATMENT ON THE STRUCTURES AND MAGNETIC PROPERTIES OF THE $\text{Co}_2\text{FeSi}_{1-x}\text{Ga}_x$ ALLOY SYSTEM.....	30
4.2.1 EFFECTS OF HEAT TREATMENT ON THE STRUCTUREL PROPERTIES OF THE $\text{Co}_2\text{FeSi}_{1-x}\text{Ga}_x$ ALLOY SYSTEM.....	32
4.2.2 EFFECTS OF HEAT TREATMENT ON THE PHASE TRANSFORMATION TEMPERATURES OF THE $\text{Co}_2\text{FeSi}_{1-x}\text{Ga}_x$ ALLOY SYSTEM.....	41
4.2.3 EFFECTS OF HEAT TREATMENT ON THE MAGNETIC PROPERTIES $\text{Co}_2\text{FeSi}_{1-x}\text{Ga}_x$ ALLOY SYSTEM.....	49
5. CONCLUSIONS	61
REFERENCES.....	63

APPENDICES

A. EDX ANALYSES OF $\text{Co}_2\text{FeSi}_{1-x}\text{Ga}_x$ ALLOY SYSTEM.....	67
B. VEGARD'S LAW	74
C. THERMAL ANALYSES OF $\text{Co}_2\text{FeSi}_{1-x}\text{Ga}_x$ ALLOY SYSTEM.....	75

LIST OF TABLES

TABLES

Table 2.1 Site occupancy, general formula, different notations (ICSD, SB, Pearson) and space group is given for different atomic order of Heusler alloys.	6
Table 4.1 Nominal and actual compositions for investigated as-cast $\text{Co}_2\text{FeSi}_{1-x}\text{Ga}_x$ ($x=0, 0.2, 0.4, 0.6, 0.8$ and 1) alloy system in at. %	19
Table 4.2 Nominal and actual compositions for the heat treated $\text{Co}_2\text{FeSi}_{1-x}\text{Ga}_x$ ($x=0, 0.2, 0.4, 0.6, 0.8$ and 1) alloy system in at.%	19
Table 4.3 Transition temperatures acquired from DSC measurements the Curie temperature, the order-order structural transition temperature from the $L2_1$ phase to the B2 phase and the melting temperature are denoted with T_c , $T_{L2_1/B2}$ and T_m for $\text{Co}_2\text{FeSi}_{1-x}\text{Ga}_x$ ($x=0, 0.2, 0.4, 0.6, 0.8$ and 1) alloy system	22
Table 4.4 Magnetic properties of the as-cast $\text{Co}_2\text{FeSi}_{1-x}\text{Ga}_x$ ($x=0, 0.2, 0.4, 0.6, 0.8$ and 1) alloy system.....	24
Table 4.5 The heat treatment temperatures and times for $\text{Co}_2\text{FeSi}_{1-x}\text{Ga}_x$ ($x=0, 0.2, 0.4, 0.6, 0.8$ and 1) alloy system.....	31
Table 4.6 The Curie temperatures, the $L2_1/B2$ order-disorder transition temperatures and the melting points for the as-cast and annealed $\text{Co}_2\text{FeSi}_{1-x}\text{Ga}_x$ ($x=0, 0.2, 0.4, 0.6, 0.8$ and 1) alloy system.....	43
Table 4.7 Magnetic properties measured at RT for the as-cast and annealed $\text{Co}_2\text{FeSi}_{1-x}\text{Ga}_x$ ($x=0, 0.2, 0.4, 0.6, 0.8$ and 1) alloy system. saturation magnetization	

and remanent magnetization are denoted by M_s (emu g^{-1}) and M_r (emu g^{-1}) respectively..... 50

LIST OF FIGURES

FIGURES

Figure 2.1 Crystal structure of Heusler alloys.	4
Figure 2.2 The many Heusler alloys can be formed by combination of the different elements according to the color scheme in the periodic table [16].	5
Figure 2.3 Crystal structure of the Heusler structure [22]	7
Figure 2.4 The calculated XRD patterns for the A2, B2, DO ₃ and L2 ₁ structures [23]	8
Figure 2.5 Hysteresis Loop	12
Figure 2.6 Magnet Types	13
Figure 2.7 Schematic representation of the density of states for a half-metallic ferromagnets.....	14
Figure 4.1 XRD patterns measured at RT for the as-cast Co ₂ FeSi _{1-x} Ga _x (x=0, 0.2, 0.4, 0.6, 0.8 and 1) alloy systems.	21
Figure 4.2 DSC patterns of the as-cast Co ₂ FeSi _{1-x} Ga _x (x=0, 0.2, 0.4, 0.6, 0.8 and 1) alloy system, obtained at rate of 10° C/min.....	23
Figure 4.3 M vs H curve measured at RT for the as-cast Co ₂ FeSi alloy, insert displays the curve in more detail.....	25
Figure 4.4 M vs H curve measured at RT for the as-cast Co ₂ FeSi _{0.8} Ga _{0.2} alloy, insert displays the curve in more detail.....	25

Figure 4.5 M vs H curve measured at RT for the as-cast $\text{Co}_2\text{FeSi}_{0.6}\text{Ga}_{0.4}$ alloy, insert displays the curve in more detail.....	26
Figure 4.6 M vs H curve measured at RT for the as-cast $\text{Co}_2\text{FeSi}_{0.4}\text{Ga}_{0.6}$ alloy, insert displays the curve in more detail.....	26
Figure 4.7 M vs H curve measured at RT for the as-cast $\text{Co}_2\text{FeSi}_{0.2}\text{Ga}_{0.8}$ alloy, insert displays the curve in more detail.....	27
Figure 4.8 M vs H curve measured at RT for the as-cast Co_2FeGa alloy, insert displays the curve in more detail.....	27
Figure 4.9 M vs H curve measured at RT for the as-cast $\text{Co}_2\text{FeSi}_{1-x}\text{Ga}_x$ ($x=0, 0.2, 0.4, 0.6, 0.8$ and 1) alloy system.....	28
Figure 4.10 M_s vs x for the as-cast $\text{Co}_2\text{FeSi}_{1-x}\text{Ga}_x$ ($x=0, 0.2, 0.4, 0.6, 0.8$ and 1) alloy system.....	29
Figure 4.11 XRD pattern measured at RT for $\text{Co}_2\text{FeSi}_{1-x}\text{Ga}_x$ ($x=0, 0.2, 0.4, 0.6, 0.8$ and 1) alloy system heat treated at 1027°C for 20 days.....	33
Figure 4.12 XRD pattern measured at RT for $\text{Co}_2\text{FeSi}_{1-x}\text{Ga}_x$ ($x=0, 0.2, 0.4, 0.6, 0.8$ and 1) alloy system annealed at $(T_{L2_1/B2} + 40^\circ\text{C})$ for 5 days.....	34
Figure 4.13 XRD pattern measured at RT for $\text{Co}_2\text{FeSi}_{1-x}\text{Ga}_x$ ($x=0, 0.2, 0.4, 0.6, 0.8$ and 1) alloy system heat treated at $(T_{L2_1/B2} - 100^\circ\text{C})$ for 5 days.	35
Figure 4.14 XRD patterns measured at RT for Co_2FeSi alloy heat treated at 950°C for 5 days, 1027°C for 20 days and 1150°C for 5 days.....	36
Figure 4.15 XRD patterns measured at RT for $\text{Co}_2\text{FeSi}_{0.8}\text{Ga}_{0.2}$ alloy heat treated at 960°C ($T_{L2_1/B2} - 100^\circ\text{C}$) for 5 days, 1027°C for 20 days and 1100°C ($T_{L2_1/B2} + 40^\circ\text{C}$) for 5 days.....	38

Figure 4.16 XRD patterns measured at RT for $\text{Co}_2\text{FeSi}_{0.6}\text{Ga}_{0.4}$ alloy heat treated at 900°C ($T_{L2_1/B2} - 100^\circ\text{C}$) for 5 days, 1027°C for 20 days and 1040°C ($T_{L2_1/B2} + 40^\circ\text{C}$) for 5 days.....	38
Figure 4.17 XRD patterns measured at RT for $\text{Co}_2\text{FeSi}_{0.4}\text{Ga}_{0.6}$ alloy heat treated at 850°C ($T_{L2_1/B2} - 100^\circ\text{C}$) for 5 days, 990°C ($T_{L2_1/B2} + 40^\circ\text{C}$) for 5 days, and 1027°C for 20 days.....	39
Figure 4.18 XRD patterns measured at RT for $\text{Co}_2\text{FeSi}_{0.2}\text{Ga}_{0.8}$ alloy annealed at 790°C ($T_{L2_1/B2} - 100^\circ\text{C}$) for 5 days, 930°C ($T_{L2_1/B2} + 40^\circ\text{C}$) for 5 days, and 1027°C for 20 days.....	40
Figure 4.19 DSC patterns of the $\text{Co}_2\text{FeSi}_{1-x}\text{Ga}_x$ ($x=0, 0.2, 0.4, 0.6, 0.8$ and 1) alloy system annealed at 1027°C for 20 days, obtained at a heating rate of $10^\circ\text{C}/\text{min}$...	44
Figure 4.20 DSC patterns of the $\text{Co}_2\text{FeSi}_{1-x}\text{Ga}_x$ ($x=0, 0.2, 0.4, 0.6, 0.8$ and 1) alloy system annealed at ($T_{L2_1/B2} + 40^\circ\text{C}$) for 5 days, obtained at a heating rate of $10^\circ\text{C}/\text{min}$	45
Figure 4.21 DSC patterns of $\text{Co}_2\text{FeSi}_{1-x}\text{Ga}_x$ ($x=0, 0.2, 0.4, 0.6, 0.8$ and 1) alloy system annealed at ($T_{L2_1/B2} - 100^\circ\text{C}$) for 5 days, obtained at a heating rate of $10^\circ\text{C}/\text{min}$	46
Figure 4.22 Composition dependence of T_c and $T_{L2_1/B2}$ $\text{Co}_2\text{FeSi}_{1-x}\text{Ga}_x$ ($x=0, 0.2, 0.4, 0.6, 0.8$ and 1) alloy system annealed at 1027°C for 20 days	48
Figure 4.23 Magnetization of the $\text{Co}_2\text{FeSi}_{1-x}\text{Ga}_x$ ($x=0, 0.2, 0.4, 0.6, 0.8$ and 1) alloy system annealed at 1027°C for 20 days as a function of magnetic field measured at RT.....	51
Figure 4.24 Magnetization of the $\text{Co}_2\text{FeSi}_{1-x}\text{Ga}_x$ ($x=0, 0.2, 0.4, 0.6, 0.8$ and 1) alloy system annealed at ($T_{L2_1/B2} + 40^\circ\text{C}$) for 5 days as a function of magnetic field measured at RT	52

Figure 4.25 Magnetization of the $\text{Co}_2\text{FeSi}_{1-x}\text{Ga}_x$ ($x=0, 0.2, 0.4, 0.6, 0.8$ and 1) alloy system annealed at $(T_{L2_1/B2}-100^\circ\text{C})$ for 5 days as a function of magnetic field measured at RT	53
Figure 4.26 Magnetization curves of the Co_2FeSi alloy annealed at 950°C for 5 days, 1027°C for 20 days and 1150°C for 5 days as a function of magnetic field measured at RT	55
Figure 4.27 Magnetization curves of the $\text{Co}_2\text{FeSi}_{0.8}\text{Ga}_{0.2}$ alloy annealed at 960°C ($T_{L2_1/B2}-100^\circ\text{C}$) for 5 days, 1027°C for 20 days and 1100°C ($T_{L2_1/B2}+40^\circ\text{C}$) for 5 days as a function of magnetic field measured at RT	56
Figure 4.28 Magnetization curves of the $\text{Co}_2\text{FeSi}_{0.6}\text{Ga}_{0.4}$ alloy annealed at 900°C ($T_{L2_1/B2}-100^\circ\text{C}$) for 5 days, 1027°C for 20 days and 1040°C ($T_{L2_1/B2}+40^\circ\text{C}$) for 5 days as a function of magnetic field measured at RT	57
Figure 4.29 Magnetization curves of the $\text{Co}_2\text{FeSi}_{0.4}\text{Ga}_{0.6}$ alloy annealed at 850°C ($T_{L2_1/B2}-100^\circ\text{C}$) for 5 days, 990°C ($T_{L2_1/B2}+40^\circ\text{C}$) for 5 days, and 1027°C for 20 days as a function of magnetic field measured at RT	58
Figure 4.30 Magnetization curves of the $\text{Co}_2\text{FeSi}_{0.2}\text{Ga}_{0.8}$ alloy annealed at 790°C ($T_{L2_1/B2}-100^\circ\text{C}$) for 5 days, 930°C ($T_{L2_1/B2}+40^\circ\text{C}$) for 5 days, and 1027°C for 20 days as a function of magnetic field measured at RT	59
Figure 4.31 Magnetization curves of the Co_2FeGa alloy annealed at 685°C ($T_{L2_1/B2}-100^\circ\text{C}$) for 5 days, 830°C ($T_{L2_1/B2}+40^\circ\text{C}$) for 5 days as a function of magnetic field measured at RT	60
Figure A.1 EDX spectrum of the as-cast Co_2FeSi alloy	67
Figure A.2 EDX spectrum for the as-cast $\text{Co}_2\text{FeSi}_{0.8}\text{Ga}_{0.2}$ alloy.....	68
Figure A.3 EDX spectrum for the as-cast $\text{Co}_2\text{FeSi}_{0.6}\text{Ga}_{0.4}$ alloy.....	68

Figure A.4 EDS spectrum for the as-cast $\text{Co}_2\text{FeSi}_{0.4}\text{Ga}_{0.6}$ alloy	69
Figure A.5 EDS spectrum for the as-cast $\text{Co}_2\text{FeSi}_{0.2}\text{Ga}_{0.8}$ alloy.....	69
Figure A.6 EDS spectrum for the as-cast Co_2FeGa alloy	70
Figure A.7 EDS spectrum of the annealed Co_2FeSi alloy.....	70
Figure A.8 EDS spectrum of the annealed $\text{Co}_2\text{FeSi}_{0.8}\text{Ga}_{0.2}$ alloy.....	71
Figure A.9 EDS spectrum of the annealed $\text{Co}_2\text{FeSi}_{0.6}\text{Ga}_{0.4}$ alloy.....	71
Figure A.10 EDS spectrum of the annealed $\text{Co}_2\text{FeSi}_{0.8}\text{Ga}_{0.6}$ alloy.....	72
Figure A.11 EDS spectrum of the annealed $\text{Co}_2\text{FeSi}_{0.2}\text{Ga}_{0.8}$ allo.....	72
Figure A.12 EDS spectrum of the annealed Co_2FeGa alloy.....	73
Figure C.1 DSC measurement for the Co_2FeSi alloy	75
Figure C.2 DSC measurement for the $\text{Co}_2\text{FeSi}_{0.8}\text{Ga}_{0.2}$ alloy	76
Figure C.3 DSC measurement for the $\text{Co}_2\text{FeSi}_{0.6}\text{Ga}_{0.4}$ alloy	76
Figure C.4 DSC measurement for the $\text{Co}_2\text{FeSi}_{0.4}\text{Ga}_{0.6}$ alloy	77
Figure C.5 DSC measurement for the $\text{Co}_2\text{FeSi}_{0.2}\text{Ga}_{0.8}$ alloy.....	77

LIST OF SYMBOLS

T_C	Curie temperature
H	Magnetic field
M	Magnetization
T_m	Melting temperature
M_s	Saturation magnetization
T_{L2₁/B2}	L2 ₁ ↔B2 phase transition temperature
M_r	Remanent magnetization
S	Order parameter
I	Peak intensity
L_P(θ)	Lorentz polarization factor
m_(hkl)	Multiplicity factor
f	Atomic scattering factor

CHAPTER 1

INTRODUCTION

Heusler alloys are ternary intermetallics with XYZ and X_2YZ general formula. The researches on these alloys showed that there is a relation between composition, chemical order and magnetic properties of these alloys [1-3]. In addition, because of their tunable electronic structure, they can provide the design of desired device characteristics such as half-metallic ferromagnets, semiconductors and superconductors [4-7].

After the discovery of the giant magnetoresistance (GMR) effect and giant tunnel magnetoresistance (TMR) effect at room temperature, half-metallic Heusler alloys have received considerable attention because of possible information technology applications in a new multidisciplinary field of spintronic devices related magnetoelectronics. For example, the read-write head of hard-discs in computers mostly use spintronics devices. Today small and high data storage density devices are used; however, spintronics gives the property of the spin degree of freedom to conventional electronic devices which non-volatility, increased data processing speed, decreased electric power consumption and increased integration densities. Recently, the Co-based Heusler alloys have gained significant importance due to their Curie temperatures higher than room temperature, high spin polarization and high magnetization per unit cell for spintronic devices [8-12].

In addition to the ternary Co_2YZ Heusler alloys, substitutional quaternary alloys have become attractive in spintronic devices with $Co_2Cr_{1-x}Fe_xAl$ alloy [13]. The

combination of two ternary alloys (Co_2YZ and Co_2YZ^*) can improve material properties and provide new materials which may have desirable properties for industrial applications. In literature, Co_2FeGa and Co_2FeSi Heusler alloys have been investigated theoretically and experimentally; however, there is not any study related quaternary Co-Fe-Si-Ga alloy system. According to theoretical and experimental studies, as a half-metallic ferromagnet, Co_2FeSi has the highest Curie temperature and magnetic moments among the Heusler alloys [10, 14-15]. On the other hand, Co_2FeGa is not stated as a half-metallic ferromagnet and its spin polarization is not very remarkable but it is a candidate material for spintronics applications due to its high Curie temperature. However, in this study, it is suggested that the partial substitution of Si and Ga can enhance the phase stability of the L2_1 structure and magnetic properties.

The aim of present study is to synthesize quaternary $\text{Co}_2\text{FeSi}_{1-x}\text{Ga}_x$ bulk samples and investigate the effect of composition and heat treatment on phase stability and magnetic properties in Heusler type quaternary alloy system. Therefore, the quaternary $\text{Co}_2\text{FeSi}_{1-x}\text{Ga}_x$ bulk samples with the Ga composition ranging from 0 to 1 for x were produced by conventional arc melting and heat treated at various temperatures. Structural and magnetic properties of $\text{Co}_2\text{FeSi}_{1-x}\text{Ga}_x$ were investigated by X-ray diffraction (XRD), differential scanning calorimetry (DSC) and vibrating sample magnetometer (VSM) measurements.

CHAPTER 2

HEUSLER ALLOYS

Heusler type alloys were discovered by German mining and chemist Friedrich Heusler in 1903 [2]. He added Al, Sn, Sb, Bi or In as a third alloying elements to binary Cu-Mn. The most important property of the Heusler type alloy shows ferromagnetic behavior although the constituting elements are paramagnetic, diamagnetic, or antiferromagnetic. These remarkable properties of Heusler alloys have gained many magnetic properties on the materials such as magneto-optical, magneto-caloric, magneto-structural and magneto-electrical characteristics.

Heusler alloys with the $L2_1$ -type crystal structure are subjected to a magnetic transformation (*ferromagnetic* \leftrightarrow *paramagnetic*) at Curie temperature and relatively high temperature atomic ordering (*order* \leftrightarrow *order* and *order* \leftrightarrow *disorder*) transformations.

2.1 THE FULL HEUSLER ($L2_1$ TYPE) STRUCTURE

There are two kinds of Heusler alloys: the full Heusler alloys and the half Heusler alloys. The first studies about Heusler alloy were materialized on the full Heusler alloy symbolized with the formula X_2YZ and Cu_2MnAl is indicated as prototype.

The full Heusler alloy crystallizes in the cubic space group $Fm\bar{3}m$ with space group no 225. X_2YZ type Heusler alloy has the completely ordered $L2_1$ type crystal

structure at room temperature. Its unit cell consists of four interpenetrating face-centered-cubic (fcc) sublattices with the Wyckoff positions (0 0 0) for X1, (1/2 1/2 1/2) for X2, (1/4 1/4 1/4) for Y and (3/4 3/4 3/4) for Z atom (Figure 2.1).

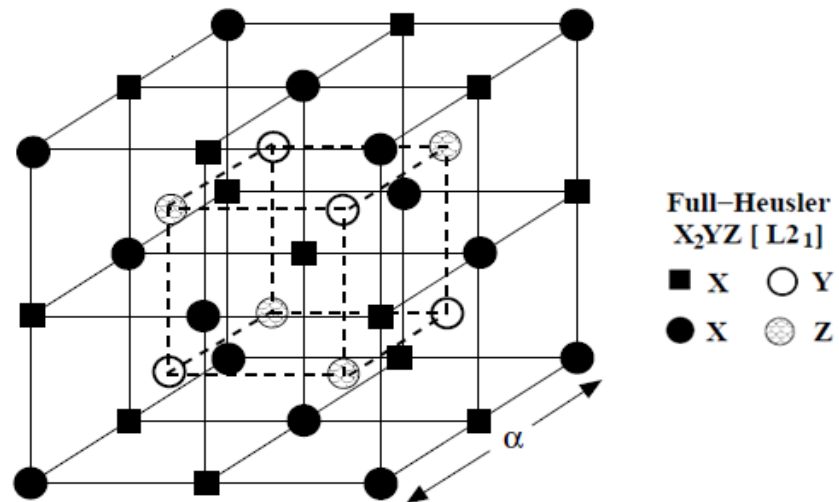


Figure 2.1 Crystal structure of Heusler alloys.

X and Y elements are typically a transition metal such as Co, Cu, Ni or Fe; Z element can be either a semiconductor or a non-magnetic metal (Al, Si, Ga, Ge, In or Sn). The possible combinations of elements to form Heusler structure is indicated in periodic table with different colours as given in Figure 2.2. While red elements indicate the X atoms, Y and Z element are shown as blue and green, respectively.

H 2.20																	He	
Li 0.98	Be 1.57											B 2.04	C 2.55	N 3.04	O 3.44	F 3.98	Ne	
Na 0.93	Mg 1.31											Al 1.61	Si 1.90	P 2.19	S 2.58	Cl 3.16	Ar	
K 0.82	Ca 1.00	Sc 1.36	Ti 1.54	V 1.63	Cr 1.66	Mn 1.55	Fe 1.83	Co 1.88	Ni 1.91	Cu 1.90	Zn 1.65	Ga 1.81	Ge 2.01	As 2.18	Se 2.55	Br 2.96	Kr 3.00	
Rb 0.82	Sr 0.95	Y 1.22	Zr 1.33	Nb 1.60	Mo 2.16	Tc 1.90	Ru 2.20	Rh 2.28	Pd 2.20	Ag 1.93	Cd 1.69	In 1.78	Sn 1.96	Sb 2.05	Te 2.10	I 2.66	Xe 2.60	
Cs 0.79	Ba 0.89			Hf 1.30	Ta 1.50	W 1.70	Re 1.90	Os 2.20	Ir 2.20	Pt 2.20	Au 2.40	Hg 1.90	Tl 1.80	Pb 1.80	Bi 1.90	Po 2.00	At 2.20	Rn
Fr 0.70	Ra 0.90																	
		La 1.10	Ce 1.12	Pr 1.13	Nd 1.14	Pm 1.13	Sm 1.17	Eu 1.20	Gd 1.20	Tb 1.10	Dy 1.22	Ho 1.23	Er 1.24	Tm 1.25	Yb 1.10	Lu 1.27		
		Ac 1.10	Th 1.30	Pa 1.50	U 1.70	Np 1.30	Pu 1.28	Am 1.13	Cm 1.28	Bk 1.30	Cf 1.30	Es 1.30	Fm 1.30	Md 1.30	No 1.30	Lr 1.30		

Figure 2.2 The many Heusler alloys can be formed by combination of the different elements according to the color scheme in the periodic table [16].

2.2 ORDER-DISORDER STRUCTURAL TRANSFORMATION

Intermetallic compounds are composed of two or more elements in stoichiometric amounts with a very narrow stability range. They have different properties from the component elements and ordered structure. Their ordered structure can be designed to develop materials for specific applications. Making a binary alloy for practical applications is easier than multicomponent alloys. When studying the multicomponent alloys, determination of the type of ordered structure and the effect of the temperature and composition on this ordering structure has significant importance.

Ordered crystal structures display significant mechanical, electrical, magnetic and physical properties. Band structure calculations demonstrate that the properties of Heusler alloys are powerfully affected by type and degree of the atomic order. A

partially disordered structure can cause serious changes in their electronic structure, magnetic and transport properties [9, 17-19].

Figure 2.3 displays the transitions from the most remarkable disordered structure to the ordered structure are displayed as in Figure 2.3 and defined in the following [20-21]. If all positions become equivalent with a bcc lattice, the X, Y and Z atoms are randomly distributed. This type disordered structure is known as A2-type structure. When the X atoms are located in (0 0 0) and (1/2 1/2 1/2) positions and Y and Z atoms are randomly sited, this partially disordered structure is known as B2-type structure. In L2₁ ordered structure, the X, Y and Z atoms are located in their lattice sites. On the contrary, if there exists the random distribution of X and Y or X and Z atoms, this conducts DO₃-type structure. Table 2.1 reviews the various ordering forms of Heusler alloys. In the table, site occupancy, general formula, space group and different notations of the crystal structures in the Inorganic Crystal Structure Database (ICSD), the Strukturberichte (SB), and the Pearson databases are given.

Table 2.1 Site occupancy, general formula, different notations (ICSD, SB, Pearson) and space group is given for different atomic order of Heusler alloys.

Site Occupancy	General Formula	ICSD	SB	Pearson	Space Group
X1=X2, Y, Z	X ₂ YZ	Cu ₂ MnAl	L2 ₁	cF16	Fm3m (no. 225)
X1=X2=Y, Z	X ₃ Z	BiF ₃	DO ₃	cF16	Fm3m (no. 225)
X1=X2, Y=Z	X ₂ Y ₂	CsCl	B2	cP2	Pm3m (no. 221)
X1=X2=Y=Z	X ₄	W	A2	cI2	Im3m (no. 229)

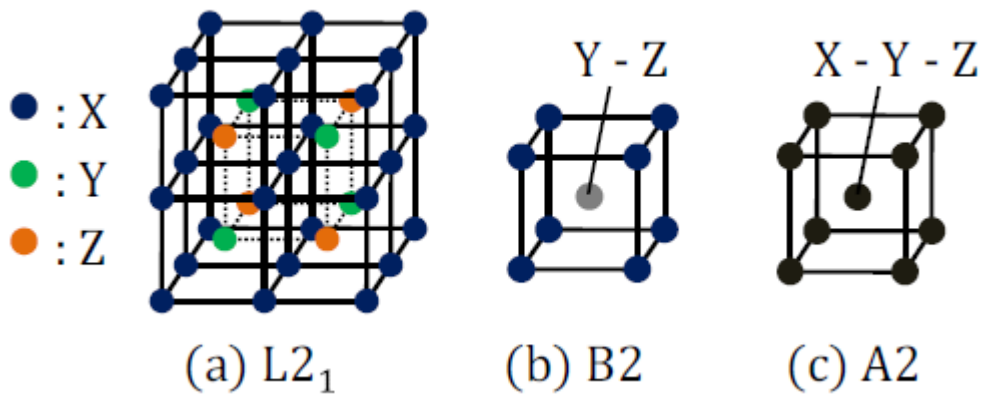


Figure 2.3 Crystal structure of the Heusler structure [22]

2.2.1. Structure Determination

In order to determine the crystal structure of Heusler alloys, powder XRD is the simplest experimental technique. In the XRD analysis, the existence of superlattice peaks, (111) and (200), and the fundamental peak (220) are focused. The presence of both superlattice peaks and the fundamental peaks indicate the formation of full Heusler alloys, $L2_1$ crystal structure, in the material. In DO_3 -type structure, because both $L2_1$ and DO_3 are in same space group, similar XRD pattern is observed but the peak intensity of (111) is higher than the peak intensity of (200). If there exists preferential disorder, this type disorder occurs between Y and Z atoms in X_2YZ chemical formula and it is understood from the disappearance of the (111) peak. This represents the B2-type structure. In a fully disordered structure, A2-type structure, both of the superlattice peaks, (111) and (200) disappear. The characteristic peak intensities of the calculated XRD pattern of A2, B2, DO_3 and $L2_1$ structures are shown in Figure 2.4.

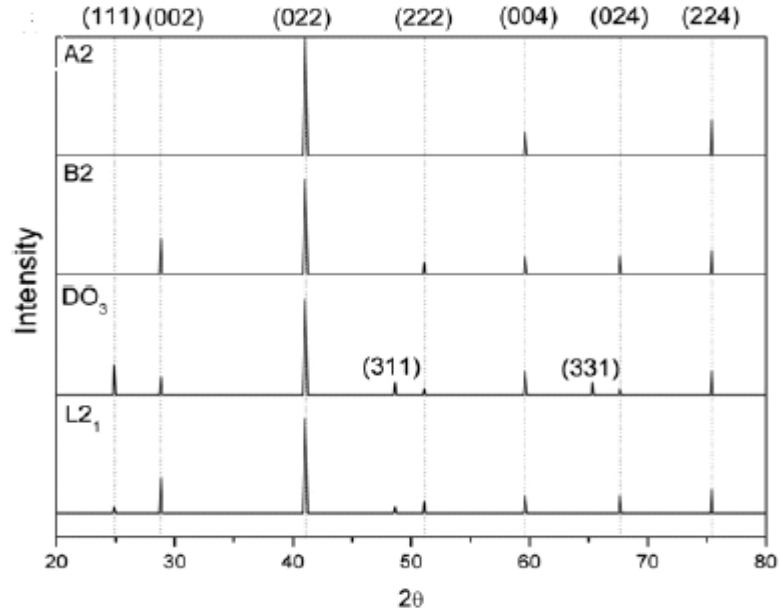


Figure 2.4 The calculated XRD patterns for the A2, B2, DO₃ and L2₁ structures [23]

The degree of atomic ordering parameter of samples can be estimated from the peak intensity of (111) and (220) reflections obtained from the XRD measurement. For this aim, the order parameter *S* is calculated by using following equation:

$$S_{L2_1}^2 = \frac{I_{obs}(111)/I_{obs}(220)}{I_{cal}(111)/I_{cal}(220)} \quad (2.1)$$

Here, *I*_{obs} and *I*_{cal} states the peak intensities obtained from the experiment and calculated, respectively. The calculated peak intensities of superlattice reflection and fundamental reflections are computed as following equation:

$$I(hkl) = |F(hkl)|^2 \cdot m_{(hkl)} L_p(\theta) \quad (2.2)$$

Here, $L_p(\theta)$ is Lorentz polarization factor, $m_{(hkl)}$ is multiplicity factor and $F(hkl)$ is the structure amplitude of the XRD diffractions for superlattice and fundamental peaks. $F(111)$, $F(200)$ and $F(220)$ are calculated by;

$$F(111) = 4|f_B - f_C| \quad (2.3)$$

$$F(200) = 4|2f_A - (f_B + f_C)| \quad (2.4)$$

$$F(220) = 4|2f_A + (f_B + f_C)| \quad (2.5)$$

where f_A , f_B and f_C are the scattering factors for the X, Y and Z atoms.

The fundamental peak (220) answer the relation $(h+k+l)/2=2n$ and is not influenced by the atomic disorder. Here h , k , l Miller indices and n is integer number. The superlattice peaks (111) and (200) are order dependent. If there exist the Y-Z disorder, while the peak intensity of (200) is not influenced, the (111) peak is decreased by the factor S^2 . However, standart powder XRD measurements cannot be enough to detect the completely ordered or disordered, the existence of small amounts of disorder in an ordered compound or a low degree in a disordered structure for most samples since the atomic scattering value of elements sited in the same period of the periodic table is close to each other. Therefore, in order to determine the direct examination of anti-site disorder, neutron diffraction or synchrotron-based anomalous X-ray diffraction investigations are well accommodated structure determination [24-25].

2.3 MAGNETISM IN HEUSLER ALLOYS

Heusler alloys have attractive magnetic properties. In the $L2_1$ -type structure, the two X atoms occupy on the tetrahedral sites. This situation provides a magnetic interaction between the X atoms and the formation of two different magnetic

sublattice since the X_2YZ Heusler alloys display diverse magnetic properties like ferromagnetism, ferrimagnetism, Pauli paramagnetism, antiferromagnetism or half-metallic ferromagnetism.

2.3.1 Ferromagnets

The magnetic orders of most Heusler alloys are ferromagnetic and saturate in faint applied magnetic fields. Heusler alloys are metal; however, they have localized magnetic properties. Therefore, their magnetic properties are affected by both atomic disorder and changes in the electron concentration.

Webster and Ziebeck displayed the effect of the X (3d) and Z (sp) atoms on magnetic properties of Heusler alloys [26]. It was exhibited that magnetic properties is influenced by both the magnetic moment formation and the type of magnetic order so that sp electron density is principally important to form desired magnetic properties.

2.3.1.1 Related Properties

Saturation Magnetization:

In order to increase in the field direction, the magnetic induction is caused by a applied magnetic field, H. If H is increased infinitely the magnetization eventually reaches saturation at a value which is designed as M_s . This situation corresponds a condition where all the magnetic dipoles within the material are aligned in the direction of magnetic field H.

Remanence:

If the field is reduced to zero after magnetizing a magnetic material the remaining magnetization is called M_r . The remanence is used to describe the value the remaining magnetization when the field is removed after the magnetic material has

been magnetized to saturation. Therefore, the remanence becomes the upper limit for magnetizations.

Curie Temperature:

All Ferromagnets and ferrimagnets when heated to sufficiently high temperatures become paramagnetic. The transition temperature from ferromagnetic to paramagnetic behaviour is called the Curie temperature, T_c . At this temperature the permeability of the material drops sharply and both coercivity and remanence zero.

Magnetic Hysteresis:

A hysteresis loop is common method to learn about the magnetic properties of a material. It shows the relation between magnetization and the applied magnetic field. It is referred to as M-H loop. An example for M-H loop is given in Figure 2.5.

The loop is generated by measuring the magnetization of a ferromagnetic material while the magnetic field is changed. Starting with a virgin state of the material at the origin 0 induction increases along the curve to the point marked +S as the field increases from zero to maximum. The point +S is the point at which the induction no longer increases with higher magnetizing field; is known as the saturation magnetization. When magnetizing field is reduced to zero in permanent magnets most of the induction is retained. When the magnetizing field is reduced through zero to -S the induction decreases from +S to -S. In well prepared permanent magnets M_r remanent magnetization approaches the saturation induction. If the field is increased again in the positive direction, the induction passes through $-H_r$ to +S but this time not through the origin. Thus there is hysteresis between the magnetization and demagnetization curves. The two halves of the loop are generally symmetrical and form a major loop, which represent the maximum energy content, of the amount of magnetic energy that can be stored in the material.

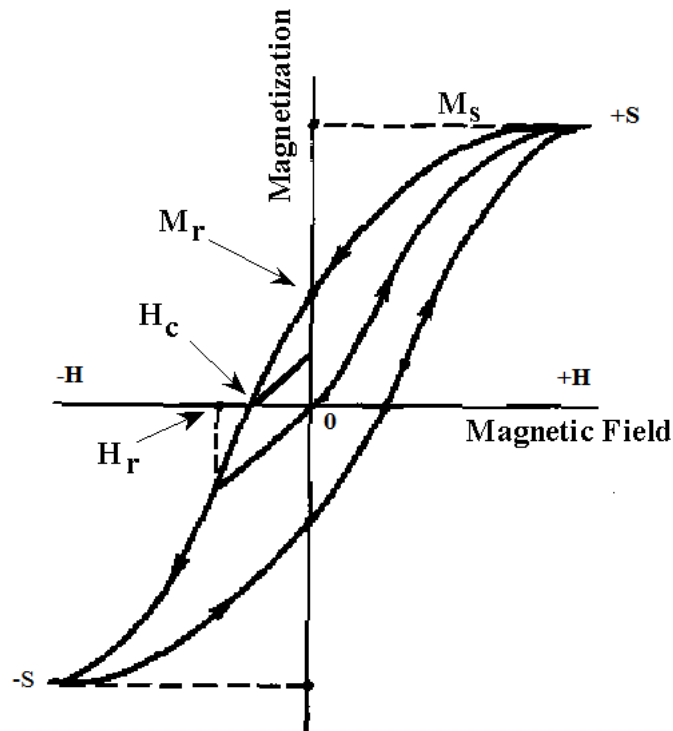


Figure 2.5 Hysteresis Loop

Magnet Types:

There are two types of magnets: hard and soft. The differences between hard and soft magnets are displayed with hysteresis loop in the most suitable way (Figure 2.6). A hard magnet attracts other magnetized materials to it. It retains the magnetism more or less permanently. A soft magnet can become magnetized and be drawn to other magnet; however, it has obvious magnetism only when it is in a magnetic field. It is not permanently magnetized.

When a magnetic material is inserted in a magnetic field, H , the adjacent lines of forces are collected into the material to increase the flux density (i.e. increased magnetic induction, M). However the increased induction is not a linear; rather, it follows a M - H relationship jumping to a high level of, and then remaining nearly constant. In a soft magnet there is a near perfect backtrack as the magnetic field is

removed. A reversed magnetic field provides a symmetrical curve in the third quadrant.

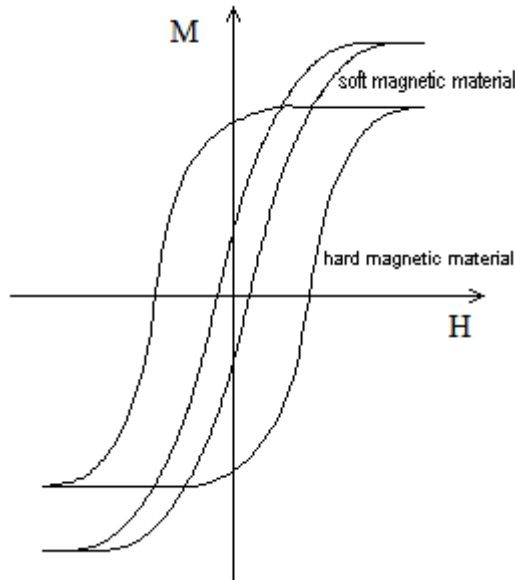


Figure 2.6 Magnet Types

Soft Magnetic Materials:

Soft magnets are the obvious choice for applications requiring ac power and high frequency operation, since they must be magnetized and demagnetized many times per second. Among the more critical specifications for soft magnets are high saturation induction, low coercive force, and maximum permeability.

2.3.2 Half-metallic Ferromagnetic

The half-metallic ferromagnetic materials have significant importance with their special electronic structure for spintronics applications. In 1983, half-metallic ferromagnetic property of half-Heusler alloy NiMnSb was discovered by de Groot and his collaborators [27]. These materials have two spin bands which display

absolutely different manner from each other. In majority band (referred as spin-up), a half-metallic ferromagnet shows the typical metallic behavior; however, in the minority spin band (referred as spin-down), it behaves like a semiconductor with a band gap at E_F , which shows that 100% spin polarization. The half-metallic ferromagnets can be assumed to be hybrids between metals and semiconductors. In Figure 2.7, a representative illustration of the density of states of a metal, a semiconductor and a half-metal is given. Due to the 100% spin polarization at the Fermi surface of the half-metal, these materials have spin polarized current. Therefore, the efficiency of spintronic devices increase. Exception of the Heusler alloys, some oxides (e.g CrO_2 and Fe_3O_4), the manganites (e.g $\text{La}_{0.7}\text{Sr}_{0.3}\text{MnO}_3$), the double perovskites (e.g $\text{Sr}_2\text{FeReO}_6$), the pyrites (e.g CoS_2), the transition metal chalcogenides (e.g CrSe) and pnictides (e.g CrAs) in the zinc-blende or wurtzite diluted magnetic semiconductors (e.g impurities in Si or GaAs) shows the half-metallic ferromagnetic properties at low temperatures. On the other hand, Heusler alloys are attractive as half-metallic ferromagnets because most of them have Curie temperature higher than room temperature.

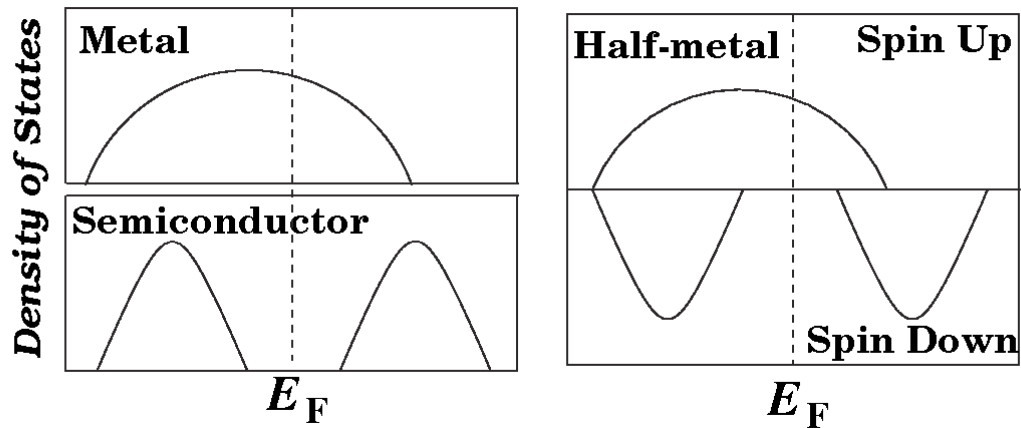


Figure 2.7 Schematic representation of the density of states for a half-metallic ferromagnets

According to electronic structure calculations, many half-metallic materials have been estimated but materials fabrication method can cause defects, structural stability, surface and interface segregation. Therefore, the half metallic property can be destroyed and spin polarization decreases.

CHAPTER 3

EXPERIMENTAL PROCEDURE

3.1 SAMPLE PREPARATION

The $\text{Co}_2\text{FeSi}_{1-x}\text{Ga}_x$ ($x=0, 0.2, 0.4, 0.6, 0.8$ and 1) polycrystalline specimens were produced by conventional arc melting method under Argon (99.7%) atmosphere to avoid oxygen contamination. The alloy were prepared by pure elements which are produced by Alfa Aesar: Co (99.9 %), Fe (99.97 %), Si (98.5 %) and Ga (99.99 %). In order to produce the desired composition, all elements were weighed. The elemental mixture were melted on the copper crucible of the arc melting. Before each melting, the arc melting chamber was evacuated to 5×10^{-5} mbar. Then, it was filled with Argon gas. Argon gas flushing was done four times. In addition to these, Zr bulk was melted to provide extra purification prior to melting the mixture. The alloy was melted three times and reversed after each melting for the sample homogeneity. Following the melting procedure, the $\text{Co}_2\text{FeSi}_{1-x}\text{Ga}_x$ bulks were cut in the form of flat disc with approximately 2 mm thickness by using precision cutting machine. Then, pieces cut from the sample were placed in an evacuated quartz tube for heat treatment. Three different heat treatments regime were applied to determine the effect of temperature on phase stability and magnetic properties. Firstly, all samples were annealed at 1150°C for 1 day and 1027°C for 20 day. This annealing temperature and time were determined from literature for Co_2FeSi [14]. Later, the other heat treatment temperatures were determined from the results of the differential

scanning calorimetry measurements of as-cast samples. According to DSC measurements, two second order transition temperatures T_c and $T_{L2_1/B2}$ were observed. The other two annealing temperatures were specified higher and lower than these $T_{L2_1/B2}$ temperatures for each composition. The annealing time was determined as 5 days from literature. For different Co-based Heusler alloys, the annealing time has been changed between three and seven day [30-33].

3.2 SAMPLE CHARACTERIZATION

X-ray Diffractometry

In order to determine the effects of composition and annealing temperature on crystal structures in the samples, X-ray diffractometry (XRD) measurements were applied. Rigaku diffractometer within CuK_α radiation was used by continuous scanning between of the diffraction angle (2θ) between 20° and 90° for XRD measurements. For powder examinations, the bulk samples were ground by hand utilizing a porcelain mortar.

Thermal Analysis

Thermal analyses of the $Co_2FeSi_{1-x}Ga_x$ samples were done by using differential scanning calorimetry method to determine the existence of magnetic ordering transition (Curie temperature, T_c) and atomic ordering transition ($L2_1$ - $B2$ order-order transformation) temperatures below the melting point. In order to determine the Curie temperature, this attempt was especially made since T_c is too high to be examined by the VSM, which is limited to $700^\circ C$. SETARAM SETSYS 16/18 differential scanning calorimeter was utilized. The samples prepared 20-30 mg were placed in high temperature Al_2O_3 crucible. Alumina powder was added in the crucible to avoid sticking sample to the crucible walls. The experiment was applied with scanning rate of $10^\circ C/ min$ under flowing high-purity argon gas atmosphere to a

temperature above the melting. Then, cooling was applied to a room temperature. As a result of DSC measurements, Curie temperature (T_C), order-disorder structural transformation temperature ($T_{L2_1/B2}$) and melting temperature (T_m) of samples were determined.

Magnetization Measurements

Magnetization measurements were done as a function of magnetic field up to 2.2 kOe by using ADE Magnetics Model EV9 Vibrating Sample Magnetometer (VSM).

Composition Analyses

The actual compositions for the as-cast and annealed $\text{Co}_2\text{FeSi}_{1-x}\text{Ga}_x$ alloys were examined by energy-dispersive X-ray spectroscopy (EDX) analyses and obtained actual values were compared with nominal values for the as-cast and the annealed alloys as tabulated in Table 4.1 and Table 4.2, respectively.

Table 4.1 Nominal and actual compositions for investigated as-cast $\text{Co}_2\text{FeSi}_{1-x}\text{Ga}_x$ ($x=0, 0.2, 0.4, 0.6, 0.8$ and 1) alloy system in at. %.

Nominal Composition	Co (at.%)	Fe (at.%)	Si (at.%)	Ga (at.%)
Co_2FeSi	49.76	26.12	24.12	-
$\text{Co}_2\text{FeSi}_{0.8}\text{Ga}_{0.2}$	49.65	26.39	19.55	4.41
$\text{Co}_2\text{FeSi}_{0.6}\text{Ga}_{0.4}$	49.96	25.87	14.20	9.97
$\text{Co}_2\text{FeSi}_{0.4}\text{Ga}_{0.6}$	50.18	26.30	9.51	14.01
$\text{Co}_2\text{FeSi}_{0.2}\text{Ga}_{0.8}$	50.53	26.37	4.37	18.73
$\text{Co}_{54}\text{Fe}_{20}\text{Ga}$	51.15	24.21	-	24.65

Table 4.2 Nominal and actual compositions for the heat treated $\text{Co}_2\text{FeSi}_{1-x}\text{Ga}_x$ ($x=0, 0.2, 0.4, 0.6, 0.8$ and 1) alloy system in at. %.

Nominal Composition	Co (at.%)	Fe (at.%)	Si (at.%)	Ga (at.%)
Co_2FeSi	49.76	26.12	24.12	-
$\text{Co}_2\text{FeSi}_{0.8}\text{Ga}_{0.2}$	49.65	26.39	19.55	4.41
$\text{Co}_2\text{FeSi}_{0.6}\text{Ga}_{0.4}$	49.96	25.87	14.20	9.97
$\text{Co}_2\text{FeSi}_{0.4}\text{Ga}_{0.6}$	50.18	26.30	9.51	14.01
$\text{Co}_2\text{FeSi}_{0.2}\text{Ga}_{0.8}$	50.77	26.56	4.43	18.23
Co_2FeGa	50.15	25.21	-	24.65

CHAPTER 4

RESULTS AND DISCUSSIONS

The $\text{Co}_2\text{FeSi}_{1-x}\text{Ga}_x$ ($x=0, 0.2, 0.4, 0.6, 0.8$ and 1) alloys have been synthesized and characterized. The results and discussions of the experimental studies on the as-cast and heat treated $\text{Co}_2\text{FeSi}_{1-x}\text{Ga}_x$ ($x=0, 0.2, 0.4, 0.6, 0.8$ and 1) alloy system have been presented individually in this chapter. Effects of composition and heat treatment on crystal structures, characteristic (atomic ordering transition and magnetic ordering) temperatures and magnetic properties have been studied for the as-cast and the heat treated $\text{Co}_2\text{FeSi}_{1-x}\text{Ga}_x$ ($x=0, 0.2, 0.4, 0.6, 0.8$ and 1) alloy system.

4.1 STRUCTURAL AND MAGNETIC PROPERTIES AND PHASE TRANSFORMATION TEMPERATURES OF AS-CAST $\text{Co}_2\text{FeSi}_{1-x}\text{Ga}_x$ ALLOY SYSTEM

The experimental results and their discussions are exhibited for the as-cast $\text{Co}_2\text{FeSi}_{1-x}\text{Ga}_x$ ($x=0, 0.2, 0.4, 0.6, 0.8$ and 1) alloy system in this section. The effects of composition on crystal structures, characteristic (atomic ordering and magnetic ordering transition) temperatures and magnetic properties were studied.

4.1.1 Effects of composition on structural properties of the as-cast $\text{Co}_2\text{FeSi}_{1-x}\text{Ga}_x$ alloy system

The as-cast $\text{Co}_2\text{FeSi}_{1-x}\text{Ga}_x$ alloys have been prepared as described in section 3.1. The effect of composition on crystal structure for the as-cast $\text{Co}_2\text{FeSi}_{1-x}\text{Ga}_x$ ($x=0, 0.2, 0.4, 0.6, 0.8$ and 1) alloy system have been demonstrated by using powder X-ray diffraction (XRD). In Figure 4.1, typical XRD patterns of the as-cast $\text{Co}_2\text{FeSi}_{1-x}\text{Ga}_x$ ($x=0, 0.2, 0.4, 0.6, 0.8$ and 1) alloy system are presented. For the as-cast $\text{Co}_2\text{FeSi}_{1-x}\text{Ga}_x$ ($x=0, 0.2, 0.4, 0.6, 0.8$ and 1) alloys, the (220), (400) and (422) are the fundamental peaks and these peaks correspond to the formation of the A2 structure in the sample. In the A2 crystal structure, all atoms Co, Fe, Si and Ga are randomly distributed on the body centered cubic lattice sites.

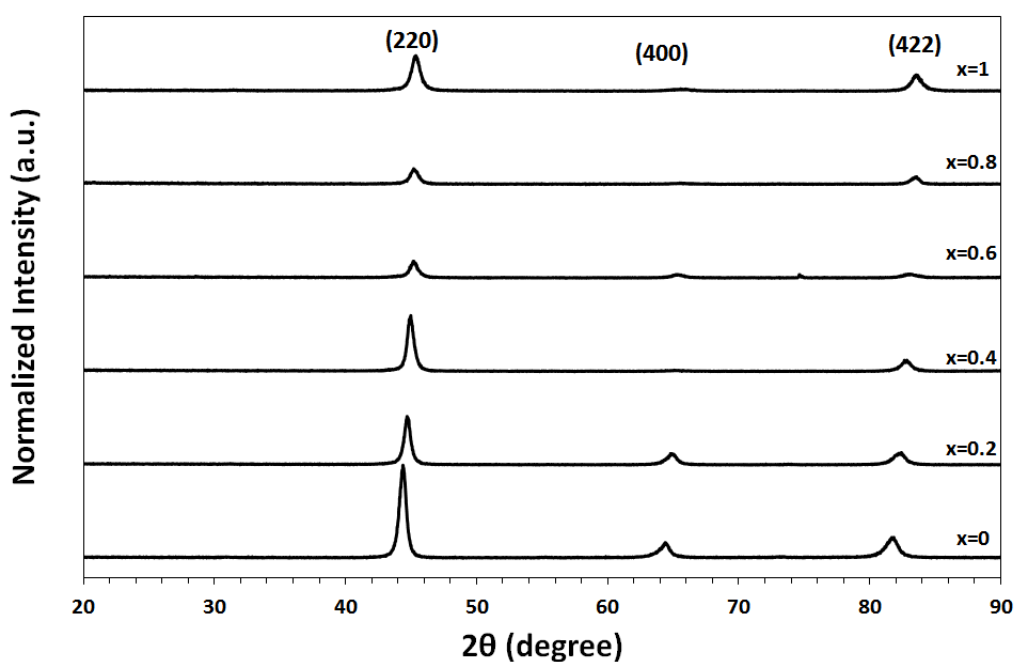


Figure 4.1 XRD patterns measured at RT for the as-cast $\text{Co}_2\text{FeSi}_{1-x}\text{Ga}_x$ ($x=0, 0.2, 0.4, 0.6, 0.8$ and 1) alloy systems.

4.1.2 Effects of composition on the phase transformation temperatures of as-cast $\text{Co}_2\text{FeSi}_{1-x}\text{Ga}_x$ alloy system

Differential scanning calorimetry (DSC) have been utilized to determine the high temperature phase transitions in $\text{Co}_2\text{FeSi}_{1-x}\text{Ga}_x$ ($x=0, 0.2, 0.4, 0.6, 0.8$ and 1) alloy system. The DSC curves of the as-cast samples obtained at a heating rate of $10^\circ\text{C}/\text{min}$ are presented in Figure 4.2. It is observed that the ferromagnetic-paramagnetic transition temperature, Curie temperature (794°C - 783°C) and the order-order atomic ordering transition temperature from the $L2_1$ phase to the B2 phase at higher temperatures can be seen from this figure. Transition temperatures obtained from DSC measurements are tabulated in Table 4.3.

Table 4.3 Transition temperatures acquired from DSC measurements the Curie temperature, the order-order structural transition temperature from the $L2_1$ phase to the B2 phase and the melting temperature are denoted with T_c , $T_{L2_1/B2}$ and T_m for $\text{Co}_2\text{FeSi}_{1-x}\text{Ga}_x$ ($x=0, 0.2, 0.4, 0.6, 0.8$ and 1) alloy system

Alloy	T_c ($^\circ\text{C}$)	$T_{L2_1/B2}$ ($^\circ\text{C}$)	T_m ($^\circ\text{C}$)
Co_2FeSi	-	768	1252
$\text{Co}_2\text{FeSi}_{0.8}\text{Ga}_{0.2}$	794	1067	1248
$\text{Co}_2\text{FeSi}_{0.6}\text{Ga}_{0.4}$	817	1003	1252
$\text{Co}_2\text{FeSi}_{0.4}\text{Ga}_{0.6}$	832	953	1256
$\text{Co}_2\text{FeSi}_{0.2}\text{Ga}_{0.8}$	833	893	1252
Co_2FeGa	783	-	1254

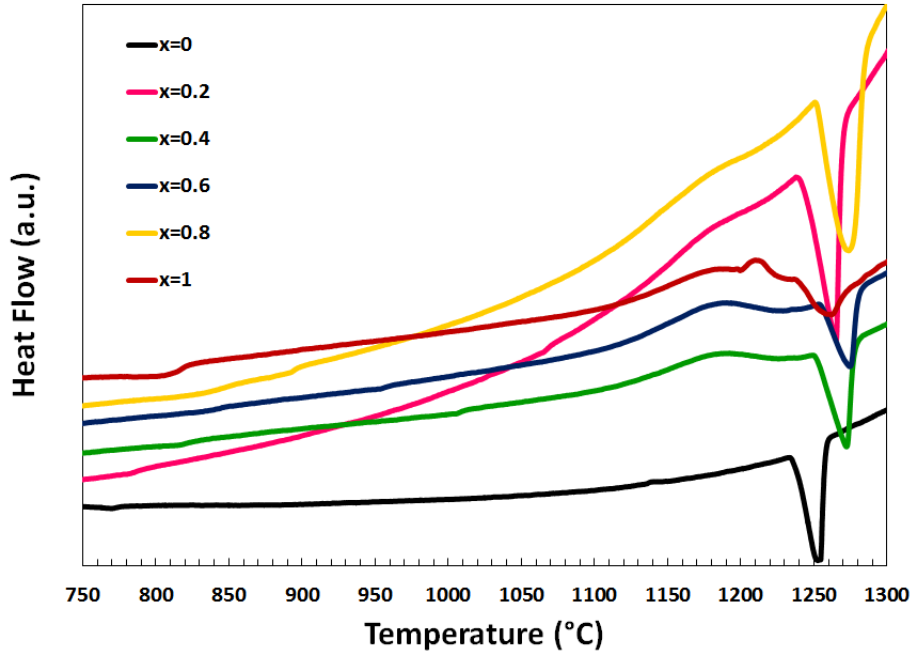


Figure 4.2 DSC patterns of the as-cast $\text{Co}_2\text{FeSi}_{1-x}\text{Ga}_x$ ($x=0, 0.2, 0.4, 0.6, 0.8$ and 1) alloy system, obtained at rate of $10^\circ\text{C}/\text{min}$.

4.1.3 Effects of composition on the magnetic properties of the as-cast $\text{Co}_2\text{FeSi}_{1-x}\text{Ga}_x$ alloy system

Individual magnetization versus magnetic field curve of each composition measured at room temperature (RT) for the as-cast $\text{Co}_2\text{FeSi}_{1-x}\text{Ga}_x$ ($x=0, 0.2, 0.4, 0.6, 0.8$ and 1) alloy system are given in Figures 4.3-4.8. In order to examine the effect of composition on the magnetization, all individual curves were plotted in a single graph (Figure 4.9). Depending on increasing in x values (range from 0 to 1), decreasing of magnetization is detected. As seen from Figures 4.3-4.8, the as-cast $\text{Co}_2\text{FeSi}_{1-x}\text{Ga}_x$ ($x=0, 0.2, 0.4, 0.6, 0.8$ and 1) alloy system behaves as strong ferromagnetic for each composition since large magnetization is observed although small magnetic field is applied for these alloys and magnetization saturates at above a certain field. Observation of ferromagnetic property may indicate the presence of

L2₁ phase as stated in Topbaşı's thesis although the ordering in the as-cast Co₂FeSi_{1-x}Ga_x alloy could not demonstrated in XRD measurements [34]. In more detail, investigated alloys are soft magnetic with a small remanance (M_r) under the experimental conditions is used here. The magnetic properties of alloys are given in table 4.4.

Table 4.4 Magnetic properties of the as-cast Co₂FeSi_{1-x}Ga_x (x=0, 0.2, 0.4, 0.6, 0.8 and 1) alloy system

Alloy	M _s (emu g ⁻¹)	M _r (emu g ⁻¹)
Co ₂ FeSi	125.074	0.187
Co ₂ FeSi _{0.8} Ga _{0.2}	121.431	0.085
Co ₂ FeSi _{0.6} Ga _{0.4}	117.498	0.114
Co ₂ FeSi _{0.4} Ga _{0.6}	112.434	0.021
Co ₂ FeSi _{0.2} Ga _{0.8}	101.949	0.025
Co ₂ FeGa	78.229	0.035

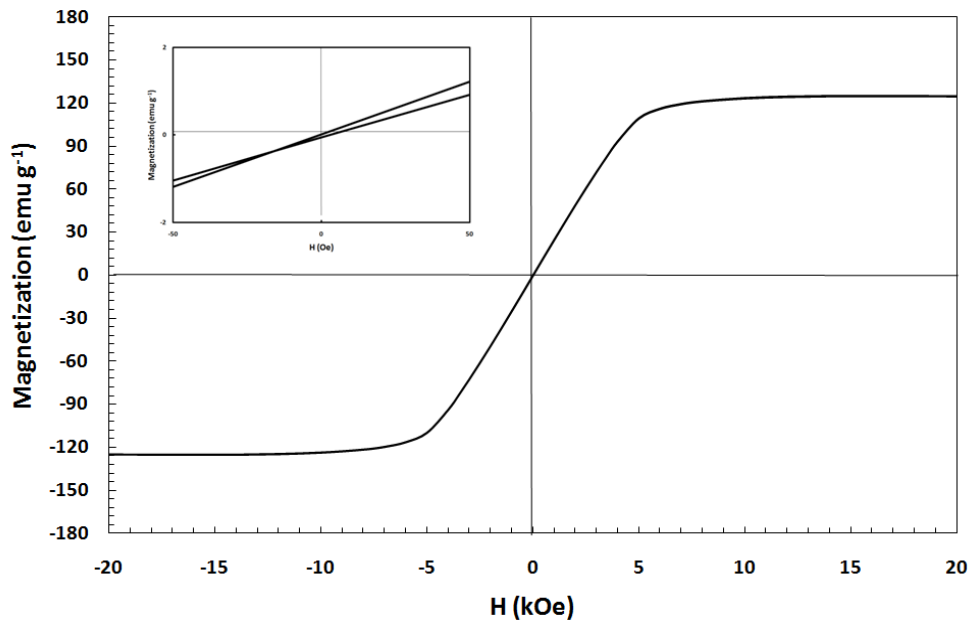


Figure 4.3 M vs H curve measured at RT for the as-cast Co_2FeSi alloy, insert displays the curve in more detail

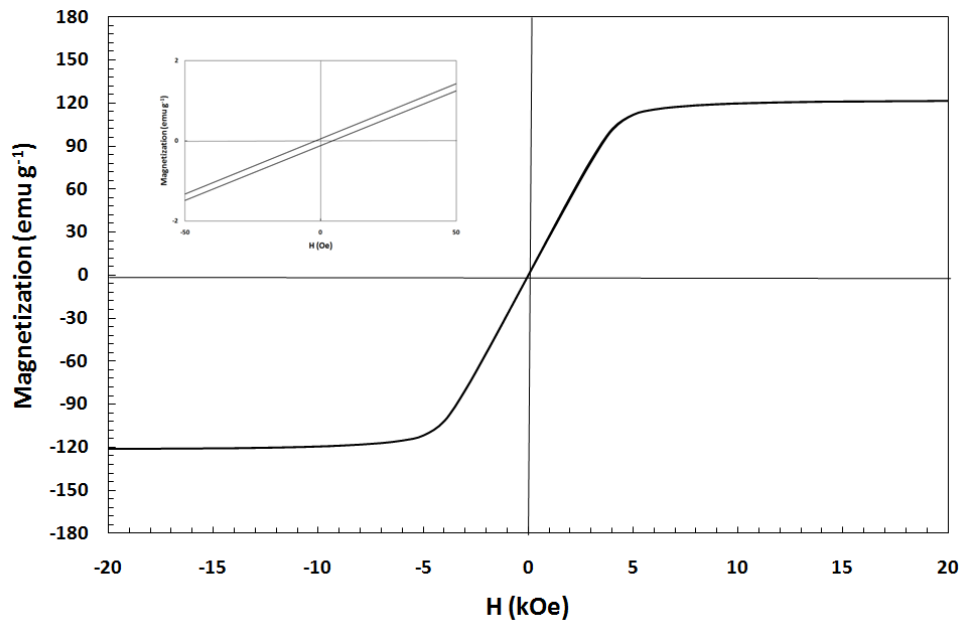


Figure 4.4 M vs H curve measured at RT for the as-cast $\text{Co}_2\text{FeSi}_{0.8}\text{Ga}_{0.2}$ alloy, insert displays the curve in more detail

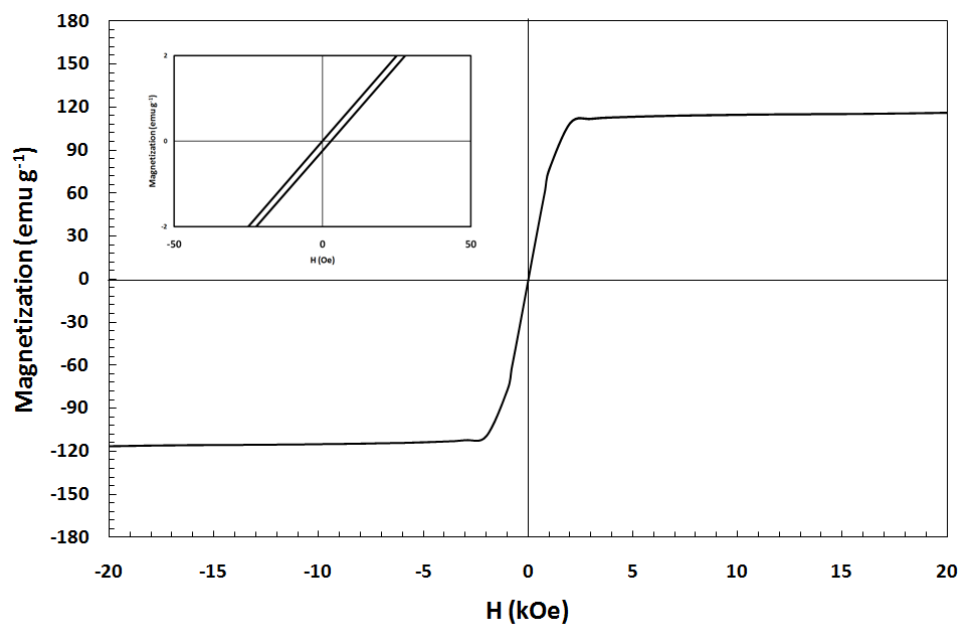


Figure 4.5 M vs H curve measured at RT for the as-cast $\text{Co}_2\text{FeSi}_{0.6}\text{Ga}_{0.4}$ alloy, insert displays the curve in more detail

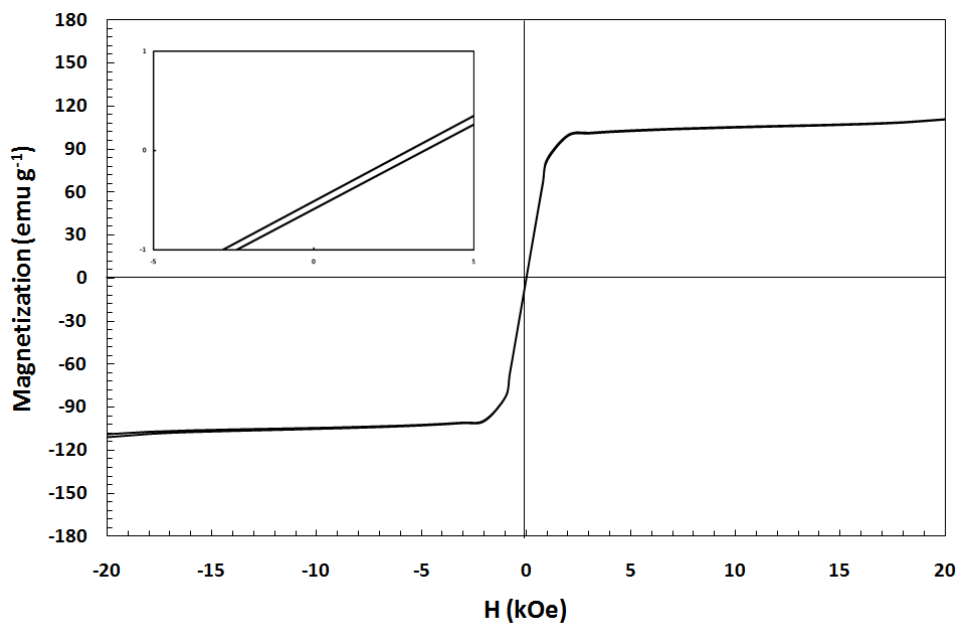


Figure 4.6 M vs H curve measured at RT for the as-cast $\text{Co}_2\text{FeSi}_{0.4}\text{Ga}_{0.6}$ alloy, insert displays the curve in more detail

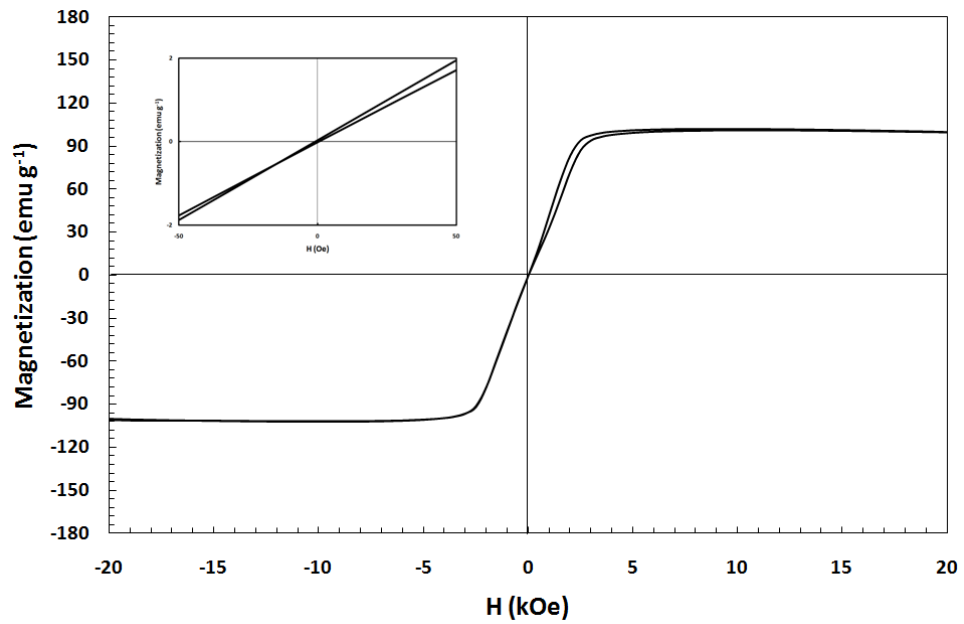


Figure 4.7 M vs H curve measured at RT for the as-cast $\text{Co}_2\text{FeSi}_{0.2}\text{Ga}_{0.8}$ alloy, insert displays the curve in more detail

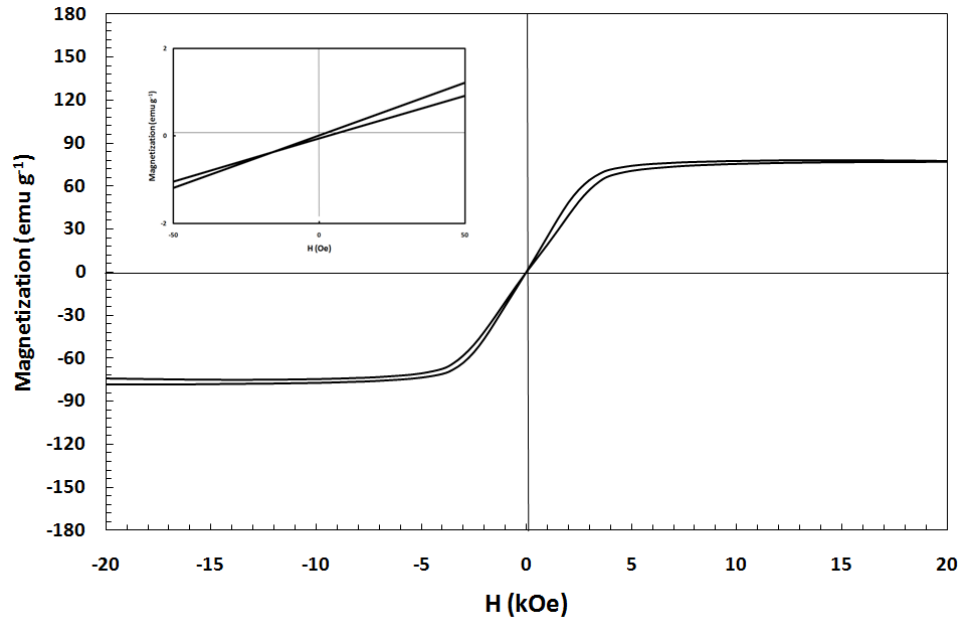


Figure 4.8 M vs H curve measured at RT for the as-cast Co_2FeGa alloy, insert displays the curve in more detail

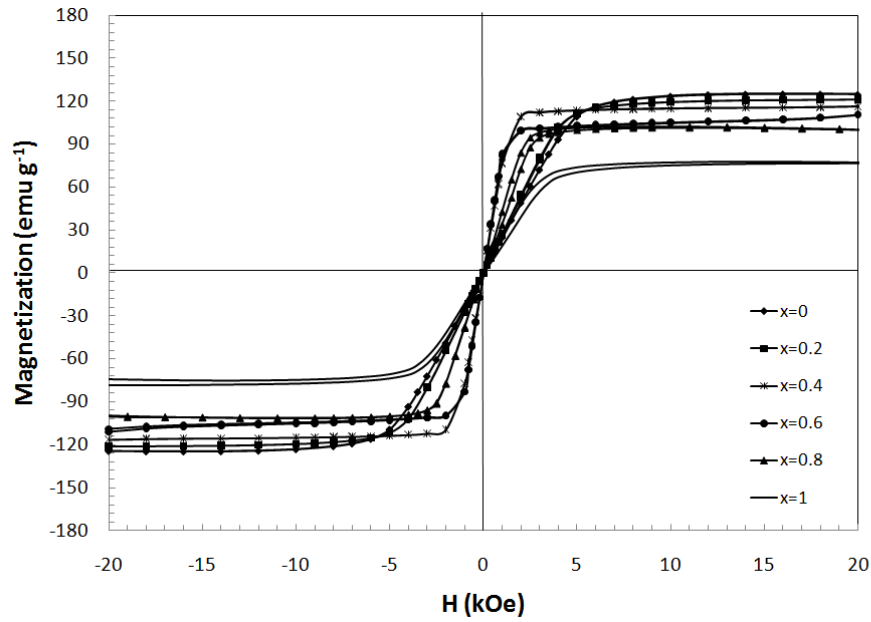


Figure 4.9 M vs H curve measured at RT for the as-cast $\text{Co}_2\text{FeSi}_{1-x}\text{Ga}_x$ ($x=0, 0.2, 0.4, 0.6, 0.8$ and 1) alloy system

Saturation magnetization M_s given as a function of Ga composition, x (at. %) in $\text{Co}_2\text{FeSi}_{1-x}\text{Ga}_x$ ($x=0, 0.2, 0.4, 0.6, 0.8$ and 1) alloy system is plotted as shown in Figure 4.10. As seen from the figure that M_s decreases with the substitution of Si with Ga in $\text{Co}_2\text{FeSi}_{1-x}\text{Ga}_x$ ($x=0, 0.2, 0.4, 0.6, 0.8$ and 1) alloy system. The substitual $\text{Co}_2\text{FeSi}_{1-x}\text{Ga}_x$ series display a nearly linear decrease of M_s with increasing Ga composition.

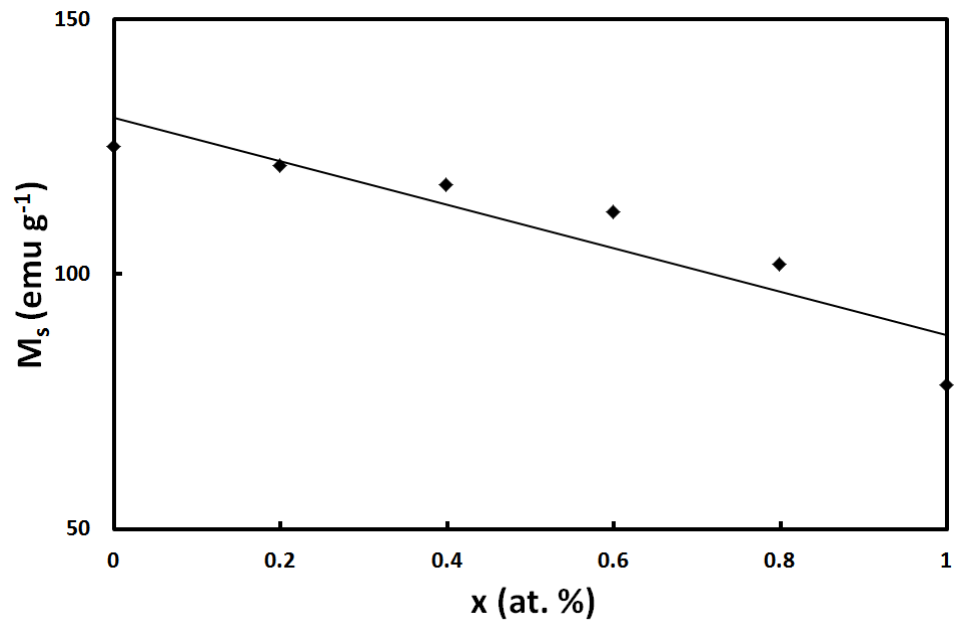


Figure 4.10 M_s vs x for the as-cast $\text{Co}_2\text{FeSi}_{1-x}\text{Ga}_x$ ($x=0, 0.2, 0.4, 0.6, 0.8$ and 1) alloy system.

4.2 EFFECT OF HEAT TREATMENT ON THE STRUCTURES AND MAGNETIC PROPERTIES OF THE $\text{Co}_2\text{FeSi}_{1-x}\text{Ga}_x$ ALLOY SYSTEM

In this part, experimental results and their discussions are covered into two part for the heat treated $\text{Co}_2\text{FeSi}_{1-x}\text{Ga}_x$ ($x=0, 0.2, 0.4, 0.6, 0.8$ and 1) alloy system. The first part presents the effects of composition on the crystal structure, characteristic (atomic ordering and magnetic ordering transition) temperature and magnetic properties. In line with the aim of this study, Co_2FeSi and Co_2FeGa alloys have been chosen as terminal alloys and four different compositions have been produced as indicated in section 3.1. The heat treatment procedure for the first group set samples were performed according to available annealing temperature and time (1027°C for 20 days) presented in the literature [14]. However, the X-ray diffraction results of I. group set samples showed that the ordering was not completed at this temperature for all alloys. Therefore, in order to investigate the effect of the heat treatment, II. and III. group set samples have been prepared and the annealing temperature have been determined according to X-ray diffraction and thermal analysis. The annealing temperatures of the samples are shown in Table 4.5. In the first group, all samples annealed at 1027°C for 20 days. For the second group heat treatment process was performed at different temperatures for each composition from 830°C to 1150°C above the $L2_1$ -B2 order-order phase transition temperature the $L2_1$ phase to the B2 phase ($T_{L2_1/B2} + 40^\circ\text{C}$) determined from DSC measurements for the I. group alloy system. Similar to second group, third group heat treatment was applied at different temperature for each composition between 685°C and 950°C below the $L2_1$ -B2 order-order phase transition temperatures ($T_{L2_1/B2} - 100^\circ\text{C}$).

Table 4.5 The heat treatment temperatures and times for $\text{Co}_2\text{FeSi}_{1-x}\text{Ga}_x$ ($x=0, 0.2, 0.4, 0.6, 0.8$ and 1) alloy system

ALLOYS	I. GROUP		II. GROUP		III. GROUP	
	$T_{\text{ann}} (^{\circ}\text{C})$	t (days)	$T_{\text{ann}} (^{\circ}\text{C})$	t (days)	$T_{\text{ann}} (^{\circ}\text{C})$	t (days)
Co_2FeSi	1027	20	1150	5	950	5
$\text{Co}_2\text{FeSi}_{0.8}\text{Ga}_{0.2}$	1027	20	1100	5	960	5
$\text{Co}_2\text{FeSi}_{0.6}\text{Ga}_{0.4}$	1027	20	1040	5	900	5
$\text{Co}_2\text{FeSi}_{0.4}\text{Ga}_{0.6}$	1027	20	990	5	850	5
$\text{Co}_2\text{FeSi}_{0.2}\text{Ga}_{0.8}$	1027	20	930	5	790	5
Co_2FeGa	1027	20	830	5	685	5

4.2.1 Effects of heat treatment on the structural properties of the heat treated $\text{Co}_2\text{FeSi}_{1-x}\text{Ga}_x$ alloy system

In order to examine the effect of composition on the crystal structures in $\text{Co}_2\text{FeSi}_{1-x}\text{Ga}_x$ ($x=0, 0.2, 0.4, 0.6, 0.8$ and 1) alloy system heat treated at 1027°C for 20 days (I. group), $T_{L2_1/B2}+40^\circ\text{C}$ for 5 days (II. group) and $T_{L2_1/B2}-100^\circ\text{C}$ for 5 days (III. group), XRD measurements were performed at room temperature as given in Figure 4.11-4.13. The superlattice peaks could not be seen; however, the inserts display that the fcc characteristic (111) and (200) peaks are obviously identified in the $\text{Co}_2\text{FeSi}_x\text{Ga}_{1-x}$ ($x=0, 0.2, 0.4, 0.6, 0.8$ and 1) alloy system.

In Figure 4.11, the first group $\text{Co}_2\text{FeSi}_{1-x}\text{Ga}_x$ ($x=0, 0.2, 0.4, 0.6, 0.8$ and 1) alloy system heat treated at 1027°C for 20 days is given. The experimental data present both the (111) and (200) peaks with nearly equal intensity indicating the long range fcc structure in the $\text{Co}_2\text{FeSi}_x\text{Ga}_{1-x}$ ($x=0, 0.2, 0.4, 0.6, 0.8$ and 1) alloy system for $x=0, 0.2$ and 0.4 . When the composition of Ga in the $\text{Co}_2\text{FeSi}_x\text{Ga}_{1-x}$ ($x=0, 0.2, 0.4, 0.6, 0.8$ and 1) alloy system is increased to a level higher than 0.4 , although Co atoms are ordered, a disorder between Fe and Si or Ga atoms are observed. This type disorder indicates the B2 type crystal structure.

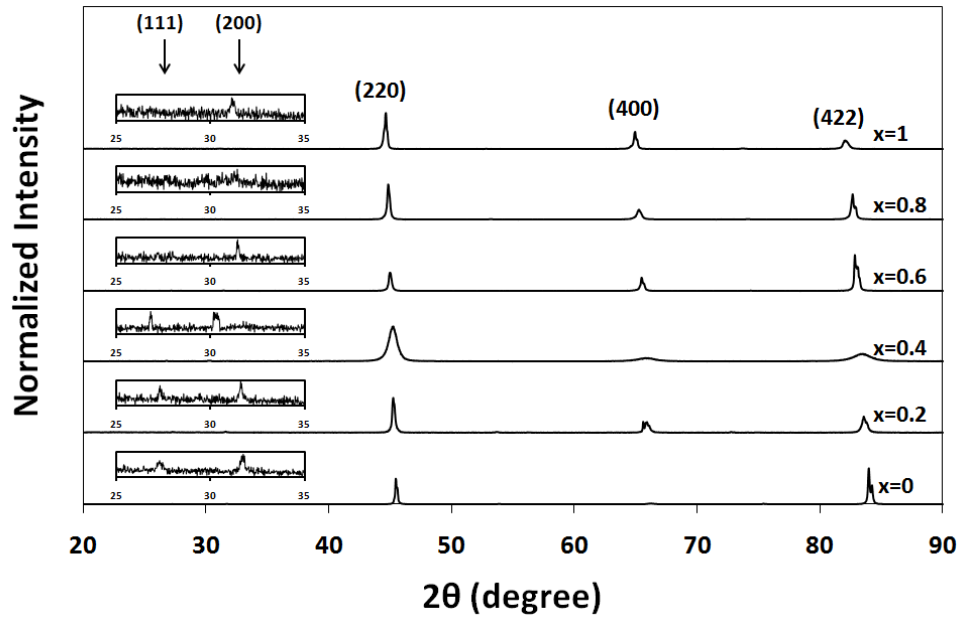


Figure 4.11 XRD pattern measured at RT for $\text{Co}_2\text{FeSi}_{1-x}\text{Ga}_x$ ($x=0, 0.2, 0.4, 0.6, 0.8$ and 1) alloy system heat treated at 1027°C for 20 days

Figure 4.12 shows the X-ray diffraction pattern of $\text{Co}_2\text{FeSi}_{1-x}\text{Ga}_x$ ($x=0, 0.2, 0.4, 0.6, 0.8$ and 1) alloy system annealed at $(T_{L2_1/B2} + 40^\circ\text{C})$ for 5 days. Annealing temperature for each composition is given in Table 4.4. The XRD patterns for $\text{Co}_2\text{FeSi}_{0.8}\text{Ga}_{0.2}$ and $\text{Co}_2\text{FeSi}_{0.6}\text{Ga}_{0.4}$ alloys exhibit the (111) and (200) peaks. The peak intensity of (111) superlattice line is higher than the peak intensity of (200) superlattice line for $\text{Co}_2\text{FeSi}_{0.8}\text{Ga}_{0.2}$ alloy. This situation probably indicates DO_3 type crystal structure. In this structure, Co and Fe atoms or Co and Si/Ga atoms are located randomly. However, determination of the exact crystal structure is not easy with conventional powder x-ray diffraction since the atomic scattering factors of elements are close to each other.

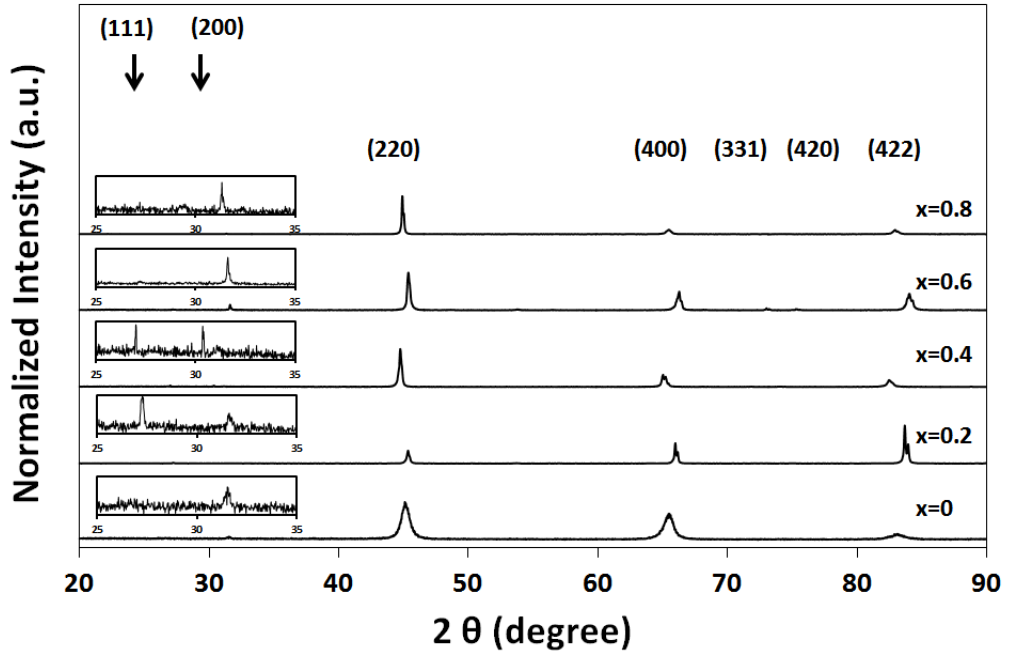


Figure 4.12 XRD pattern measured at RT for $\text{Co}_2\text{FeSi}_{1-x}\text{Ga}_x$ ($x=0, 0.2, 0.4, 0.6, 0.8$ and 1) alloy system annealed at $(T_{L2_1/B2} + 40^\circ\text{C})$ for 5 days

The XRD pattern of the $\text{Co}_2\text{FeSi}_{1-x}\text{Ga}_x$ ($x=0, 0.2, 0.4, 0.6, 0.8$ and 1) alloy system annealed below the $L2_1$ -B2 order-order phase transition temperature from the $L2_1$ phase to the B2 phase ($T_{L2_1/B2} - 100^\circ\text{C}$) are exhibited in Figure 4.13. The absence of the (111) and (200) superlattice peaks demonstrate the random distribution of Co, Fe and Si atoms for the Co_2FeSi alloy. On the contrary, the existence of the (200) superlattice peak in the $\text{Co}_2\text{FeSi}_{0.8}\text{Ga}_{0.2}$ and $\text{Co}_2\text{FeSi}_{0.6}\text{Ga}_{0.4}$ indicate that the Co atoms are ordered but Fe/ [Si, Ga] sites are disordered. This type of crystal structure represents the B2 structure. The $\text{Co}_2\text{FeSi}_{1-x}\text{Ga}_x$ alloy system with $x \geq 0.6$ has the $L2_1$ -type ordered structure, involving the (111) superlattice peak. While the (111) peak intensity for the $x=0.6$ sample is very weak, the peak intensity increase with increasing Ga content. This indicates that the degree of order enhances with increasing Ga content [32].

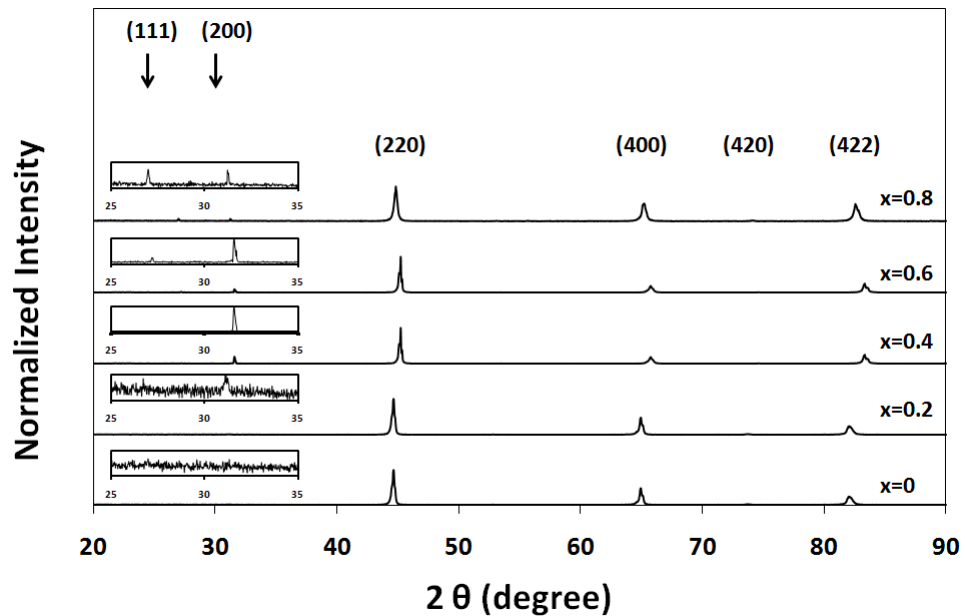


Figure 4.13 XRD pattern measured at RT for $\text{Co}_2\text{FeSi}_{1-x}\text{Ga}_x$ ($x=0, 0.2, 0.4, 0.6, 0.8$ and 1) alloy system heat treated at ($T_{L2_1/B2} - 100^\circ\text{C}$) for 5 days.

The aim of this study was to improve the structural properties by enhancing the $L2_1$ phase and determine the effect of heat treatment on the phase stability of the $L2_1$ phase. Therefore, a reference temperature for Co_2FeSi alloy was chosen from literature as first step and the $\text{Co}_2\text{FeSi}_x\text{Ga}_{1-x}$ ($x=0, 0.2, 0.4, 0.6, 0.8$ and 1) alloy system were annealed with this chosen temperature [14]. The other two temperatures were selected to be higher and lower than the order-order ($L2_1 \leftrightarrow B2$) phase transition temperature determined by DSC measurements for the I.group $\text{Co}_2\text{FeSi}_x\text{Ga}_{1-x}$ ($x=0, 0.2, 0.4, 0.6, 0.8$ and 1) alloy system. The room temperature XRD data of the $\text{Co}_2\text{FeSi}_{1-x}\text{Ga}_x$ ($x=0, 0.2, 0.4, 0.6, 0.8$ and 1) alloy system are shown in Figures 4.14-4.18.

For Co_2FeSi alloy, the heat treatment temperatures were selected randomly higher and lower than 1027°C . In Figure 4.14, XRD patterns for Co_2FeSi alloy heat treated at 950°C for, 1027°C and 1150°C are shown. XRD result of Co_2FeSi alloy heat treated at 1027°C for 20 days was consistent with literature [10], which indicates the

existence of (111) and (200) superlattice peaks that is property of the ordered L2₁ phase. It is hard to quantify the degree of long-range order parameter for the specimen since the intensities of superlattice peaks are highly faint [36]. On the other hand, it is seen that the XRD pattern of the sample heat treated at 1150°C has only (200) superlattice peak, which indicates the ordering in the Co sublattices and the disordering between Fe and Si atoms. XRD pattern for the sample heat treated at 950°C has no (111) and (200) superlattice peaks, which corresponds to the fully disordered A2 type crystal structure.

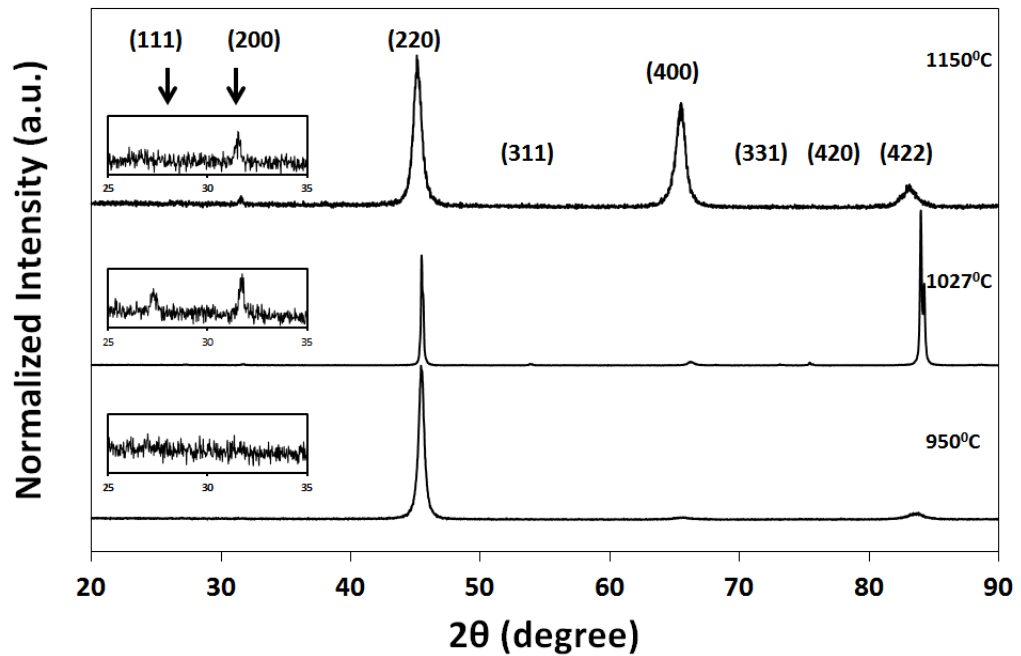


Figure 4.14 XRD patterns measured at RT for Co₂FeSi alloy heat treated at 950°C for 5 days, 1027°C for 20 days and 1150°C for 5 days

The room temperature XRD patterns for $\text{Co}_2\text{FeSi}_{0.8}\text{Ga}_{0.2}$ and $\text{Co}_2\text{FeSi}_{0.6}\text{Ga}_{0.4}$ alloys heat treated at lower than $T_{L2_1/B2}$ and higher than $T_{L2_1/B2}$ are shown in Figure 4.15 and 4.16, respectively. The order-order structural transition temperatures from the $L2_1$ phase to the B2 phase for the $\text{Co}_2\text{FeSi}_{0.8}\text{Ga}_{0.2}$ and $\text{Co}_2\text{FeSi}_{0.6}\text{Ga}_{0.4}$ alloys were determined at 1067°C and 1003°C , respectively. The XRD results of $\text{Co}_2\text{FeSi}_{0.8}\text{Ga}_{0.2}$ and $\text{Co}_2\text{FeSi}_{0.6}\text{Ga}_{0.4}$ alloys heat treated at lower than $T_{L2_1/B2}$ for 5 days show that these alloys have only (200) superlattice peak, indicating the B2 type disorder. On the contrary, the XRD patterns of the $\text{Co}_2\text{FeSi}_{0.8}\text{Ga}_{0.2}$ and $\text{Co}_2\text{FeSi}_{0.6}\text{Ga}_{0.4}$ alloys heat treated at 1027°C for 20 days exhibit both (111) and (200) superlattice peaks, which indicate the $L2_1$ type ordered structure with equivalent intensity. When the heat treatment temperature is increased over the $T_{L2_1/B2}$, both (111) and (200) superlattice peaks are observed; however, while the intensity peak of (111) is almost equal to the intensity peak of (200) for $\text{Co}_2\text{FeSi}_{0.6}\text{Ga}_{0.4}$ alloy, the intensity of (111) peak is higher than the intensity of (200) peak for $\text{Co}_2\text{FeSi}_{0.8}\text{Ga}_{0.2}$ alloy. The (111) superlattice peak with higher intensity compared to the (200) superlattice peak reported by Felser et al. could be interpreted as DO_3 type disorder [40]. When there is a partially disorder between Co and Fe atoms, X-ray diffraction could not easily distinguish this type of disorder since the scattering factors of Co and Fe transition metals are very close to each other. This conducts a similar diffraction patterns since $L2_1$ and DO_3 belongs to the identical $Fm\bar{3}m$ symmetry system.

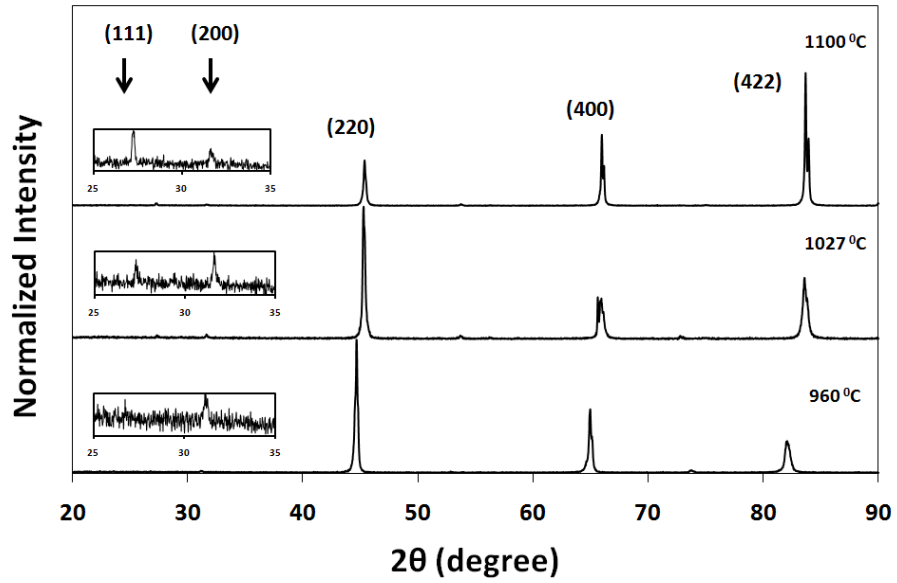


Figure 4.15 XRD patterns measured at RT for $\text{Co}_2\text{FeSi}_{0.8}\text{Ga}_{0.2}$ alloy heat treated at 960°C ($T_{L2_1/B2} - 100^\circ\text{C}$) for 5 days, 1027°C for 20 days and 1100°C ($T_{L2_1/B2} + 40^\circ\text{C}$) for 5 days

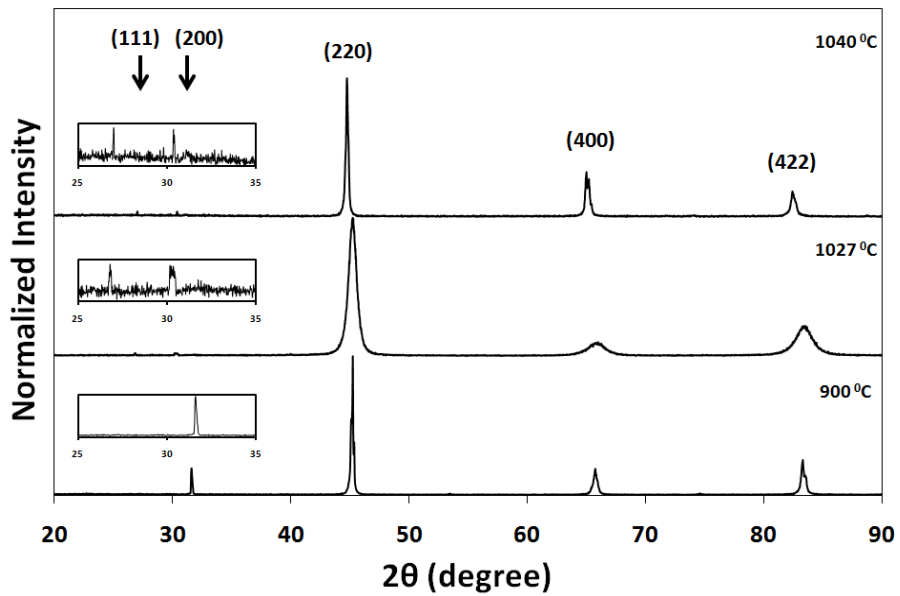


Figure 4.16 XRD patterns measured at RT for $\text{Co}_2\text{FeSi}_{0.6}\text{Ga}_{0.4}$ alloy heat treated at 900°C ($T_{L2_1/B2} - 100^\circ\text{C}$) for 5 days, 1027°C for 20 days and 1040°C ($T_{L2_1/B2} + 40^\circ\text{C}$) for 5 days

Figure 4.18 and 4.19 show, respectively, the XRD results for $\text{Co}_2\text{FeSi}_{0.4}\text{Ga}_{0.6}$ and $\text{Co}_2\text{FeSi}_{0.2}\text{Ga}_{0.8}$ alloys heat treated at lower than $T_{L_2_1/B_2}$ and higher than $T_{L_2_1/B_2}$. The XRD patterns of $\text{Co}_2\text{FeSi}_{0.4}\text{Ga}_{0.6}$ and $\text{Co}_2\text{FeSi}_{0.2}\text{Ga}_{0.8}$ alloys heat treated at lower temperature than $T_{L_2_1/B_2}$ exhibit diffractions from (111) and (200) superlattice lines those specifying L_2_1 type crystal structure. The peak intensity of (111) decreases for $\text{Co}_2\text{FeSi}_{0.4}\text{Ga}_{0.6}$ heat treated at 990°C and disappears for $\text{Co}_2\text{FeSi}_{0.4}\text{Ga}_{0.6}$ heat treated at 1027°C . The structure transforms from the L_2_1 phase to the B_2 phase with increasing annealing temperature. For $\text{Co}_2\text{FeSi}_{0.2}\text{Ga}_{0.8}$ alloy, the peak intensities of both the (111) and (200) reflections disappear respectively with increasing annealing temperature.

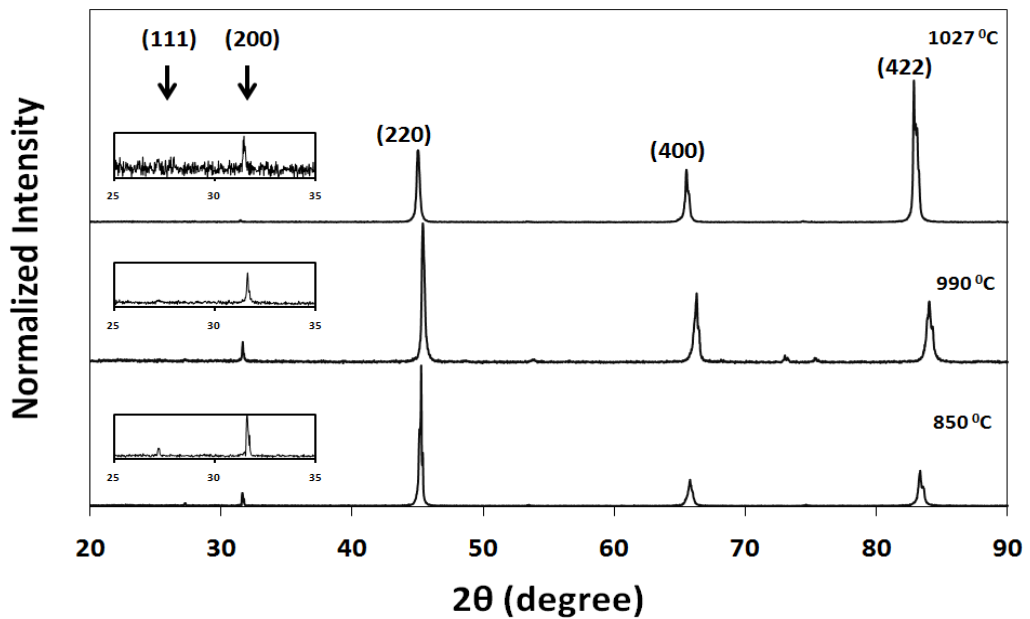


Figure 4.17 XRD patterns measured at RT for $\text{Co}_2\text{FeSi}_{0.4}\text{Ga}_{0.6}$ alloy heat treated at 850°C ($T_{L_2_1/B_2} - 100^\circ\text{C}$) for 5 days, 990°C ($T_{L_2_1/B_2} + 40^\circ\text{C}$) for 5 days, and 1027°C for 20 days

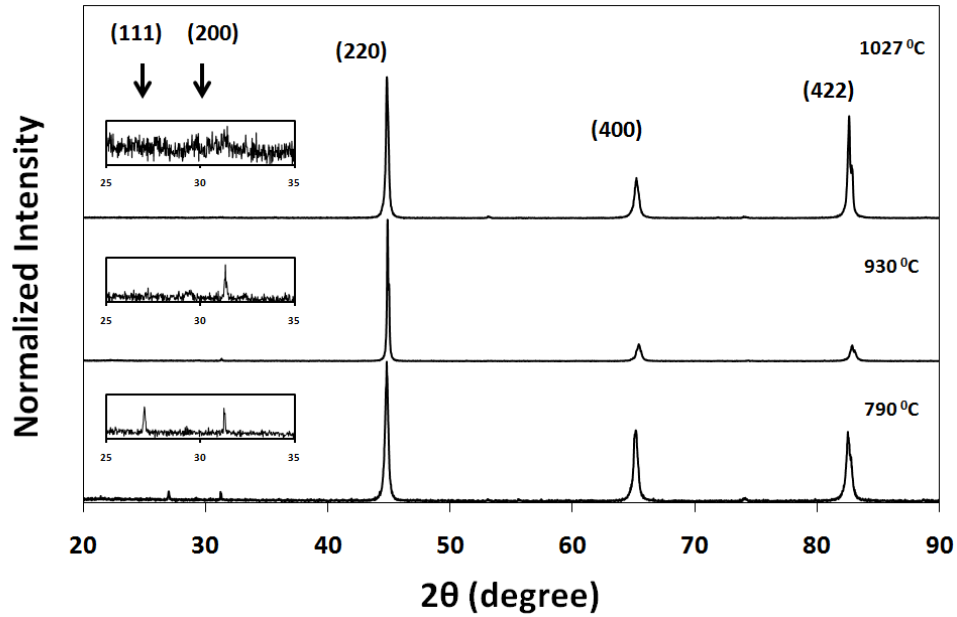


Figure 4.18 XRD patterns measured at RT for $\text{Co}_2\text{FeSi}_{0.2}\text{Ga}_{0.8}$ alloy annealed at 790°C ($T_{L2_1/B2} - 100^\circ\text{C}$) for 5 days, 930°C ($T_{L2_1/B2} + 40^\circ\text{C}$) for 5 days, and 1027°C for 20 days

The room temperature XRD patterns for $\text{Co}_2\text{FeSi}_{1-x}\text{Ga}_x$ ($x=0, 0.2, 0.4, 0.6, 0.8$ and 1) alloy system show the existence of $L2_1$, B2 and A2 type crystals structures in the effect of different heat treatments. By proper selection of composition, annealing temperature and time, the $L2_1$ phase formation is probably promoted. When two terminal compositions, Co_2FeSi and Co_2FeGa , are compared, the higher temperature and longer time is required to obtain $L2_1$ phase in the Co_2FeSi alloy than Co_2FeGa alloy. The reason of this result is that the atomic diffusivity of Si is lower than the atomic diffusivity of Ga [41]. In order to form desirable $L2_1$ phase in $\text{Co}_2\text{FeSi}_{1-x}\text{Ga}_x$ alloys with high Si concentration, high temperature and high time are required for a convenient heat treatment. The proper annealing temperature for the Ga-rich alloys is below the order-order transition temperature from the $L2_1$ phase to the B2 phase to obtain the $L2_1$ type ordered structure.

4.2.2 Effects of heat treatment on the phase transformation temperatures of the $\text{Co}_2\text{FeSi}_{1-x}\text{Ga}_x$ alloy system

In order to determine the effect of composition and heat treatment on the characteristic (atomic ordering and magnetic ordering transition) temperatures in the $\text{Co}_2\text{FeSi}_{1-x}\text{Ga}_x$ ($x=0, 0.2, 0.4, 0.6, 0.8$ and 1) alloy system, DSC measurement have been performed. The values of the Curie temperature, T_C , and the L_{2_1} - B_2 order-order transition temperature, $T_{L_{2_1}/B_2}$, for the annealed $\text{Co}_2\text{FeSi}_{1-x}\text{Ga}_x$ ($x=0, 0.2, 0.4, 0.6, 0.8$ and 1) alloy system are tabulated in Table 4.6. Figures 4.19-4.21 display the DSC heating curves of $\text{Co}_2\text{FeSi}_{1-x}\text{Ga}_x$ ($x=0, 0.2, 0.4, 0.6, 0.8$ and 1) alloy system annealed at 1027°C for 20 days, above and below the $T_{L_{2_1}/B_2}$ for 5 days, respectively. All DSC graphs show similar trend. In graph, closed triangles and squares indicate the T_C and $T_{L_{2_1}/B_2}$ respectively. While T_C increases, $T_{L_{2_1}/B_2}$ decreases with increasing Ga content. There is not a significant change in the values of T_C and $T_{L_{2_1}/B_2}$ with changing annealing temperatures (see Appendix C).

For two terminal compositions, the Curie temperature and the L_{2_1} - B_2 order-order transition temperatures are too close to each other. For Co_2FeSi Heusler alloy, Wurmehl et. al. reported that the Curie temperature was found to be $T_C = (827 \pm 20)^\circ\text{C}$ [15]. Balke et. al. was performed DSC measurements with different rates to determine the magnetic transition temperatures, T_C and the L_{2_1} - B_2 order-order transition temperature, $T_{L_{2_1}/B_2}$ for $\text{Co}_2\text{Mn}_{1-x}\text{Fe}_x\text{Si}$ alloys; however, it is impossible to distinguish nearby characteristic transition temperatures [42]. In order to overcome this problem, Kobayashi et. al. examined the Curie temperature in their study by measuring the temperature dependence of the magnetization for the $\text{Co}_2\text{Cr}_{1-x}\text{Fe}_x\text{Ga}$ [33]. They have reported that the Curie temperature, T_C and the L_{2_1} - B_2 order-order transition temperature, $T_{L_{2_1}/B_2}$ for the Co_2FeGa alloy were measured by DSC and VSM as 821°C [33, 36]. In our study, the Curie temperature and the L_{2_1} - B_2 order-

order transition temperature could not be distinguish from each other and due to the high Curie temperature; it could not be determined directly by the VSM, which is limited to 700°C even in the high temperature mode. The order-disorder phase transition temperature for the Co_2FeGa alloy and the Curie temperatures for the Co_2FeSi and Co_2FeGa alloys are slightly different from the reported studies. This deviation may be consequence of the variety in the degree of disorder caused from laboratory to laboratory in the heat treatment and quenching procedure

Table 4.6 The Curie temperatures, the L₂₁/B₂ order-disorder transition temperatures and the melting points for the as-cast and annealed Co₂FeSi_{1-x}Ga_x (x=0, 0.2, 0.4, 0.6, 0.8 and 1) alloy system

Alloy	As-cast						T _{ann} =1027°C						T _{ann} =T _{L₂₁/B₂} +40°C						T=T _{L₂₁/B₂} -100°C					
	T _C	T _{L₂₁/B₂}	T _m	T _C	T _m	T _C	T _{L₂₁/B₂}	T _m	T _C	T _m	T _C	T _{L₂₁/B₂}	T _m	T _C	T _m	T _C	T _{L₂₁/B₂}	T _m	T _C	T _{L₂₁/B₂}	T _m			
Co ₂ FeSi	-	768	1252	-	773	1253	-	771	1251	-	769	1249	-	769	1249	-	769	1249	-	769	1249	-		
Co ₂ FeSi _{0.8} Ga _{0.2}	794	1067	1248	782	1068	1247	787	1069	1246	785	1070	1247	787	1069	1246	785	1070	1247	785	1070	1247	785		
Co ₂ FeSi _{0.6} Ga _{0.4}	817	1003	1252	817	1008	1253	815	1007	1257	814	1004	1253	815	1007	1257	814	1004	1253	814	1004	1253	814		
Co ₂ FeSi _{0.4} Ga _{0.6}	832	953	1256	835	956	1259	833	956	1257	830	953	1255	833	956	1257	830	953	1255	830	953	1255	830		
Co ₂ FeSi _{0.2} Ga _{0.8}	833	892	1252	838	894	-	842	894	1256	839	893	1257	842	894	1256	839	893	1257	839	893	1257	839		
Co ₂ FeGa	783	783	1254	787	787	1257	-	-	-	-	-	-	-	-	-	-	-	-	-	-	-	-		

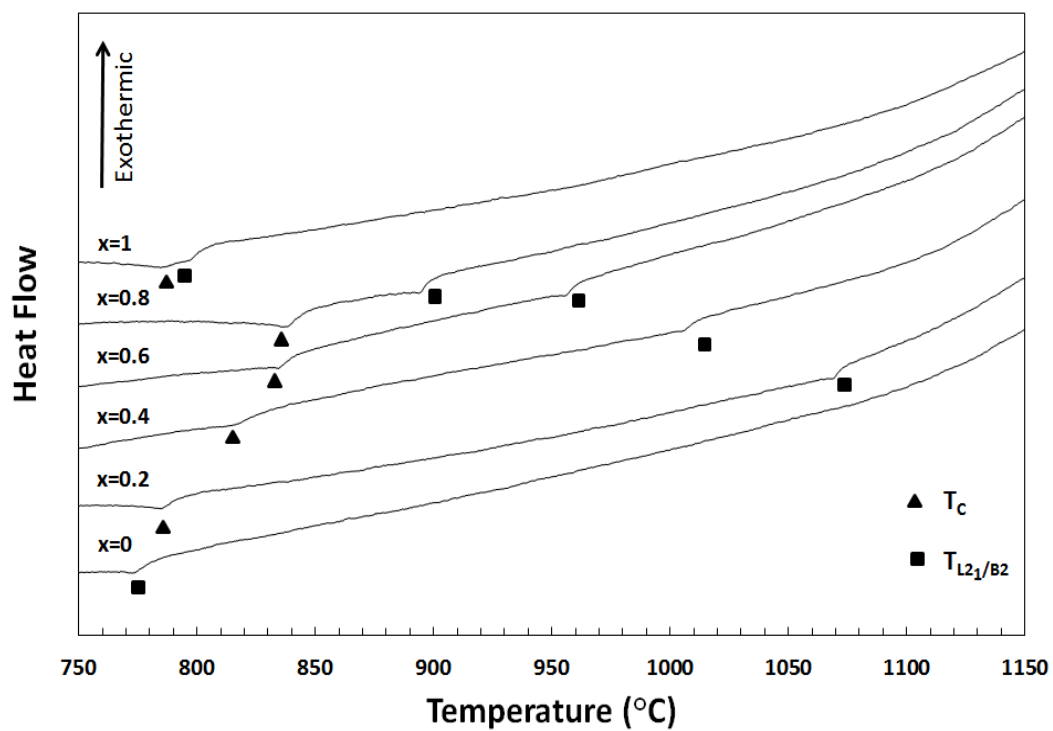


Figure 4.19 DSC patterns of the $\text{Co}_2\text{FeSi}_{1-x}\text{Ga}_x$ ($x=0, 0.2, 0.4, 0.6, 0.8$ and 1) alloy system annealed at 1027°C for 20 days, obtained at a heating rate of $10^\circ\text{C}/\text{min}$

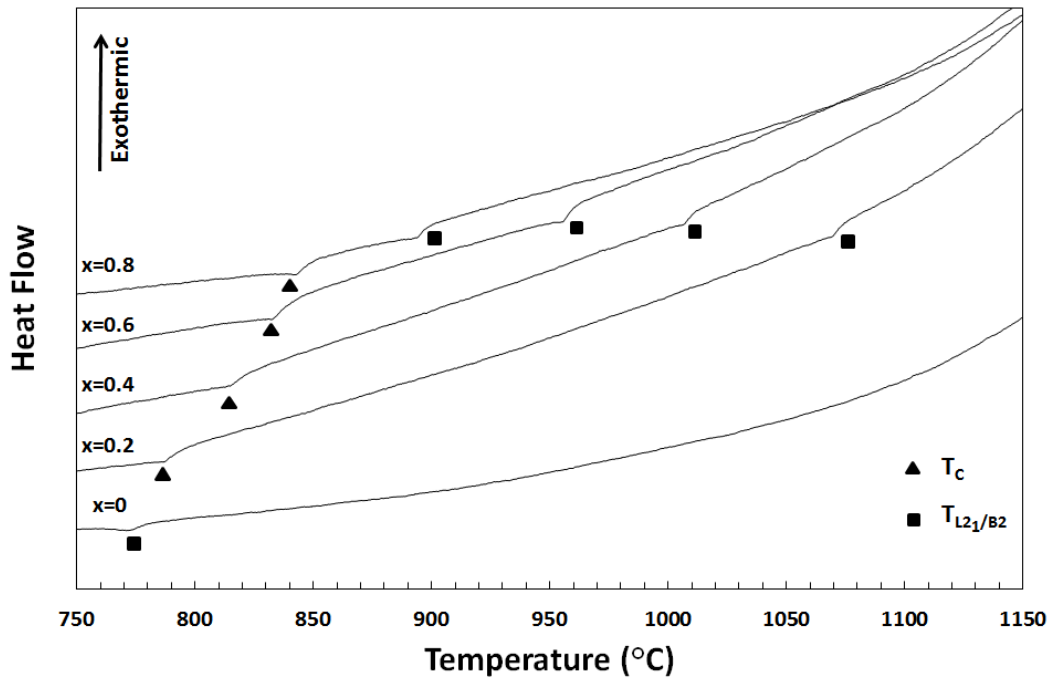


Figure 4.20 DSC patterns of the $\text{Co}_2\text{FeSi}_{1-x}\text{Ga}_x$ ($x=0, 0.2, 0.4, 0.6, 0.8$ and 1) alloy system annealed at $(T_{L2_1/B2} + 40^\circ\text{C})$ for 5 days, obtained at a heating rate of $10^\circ\text{C}/\text{min}$

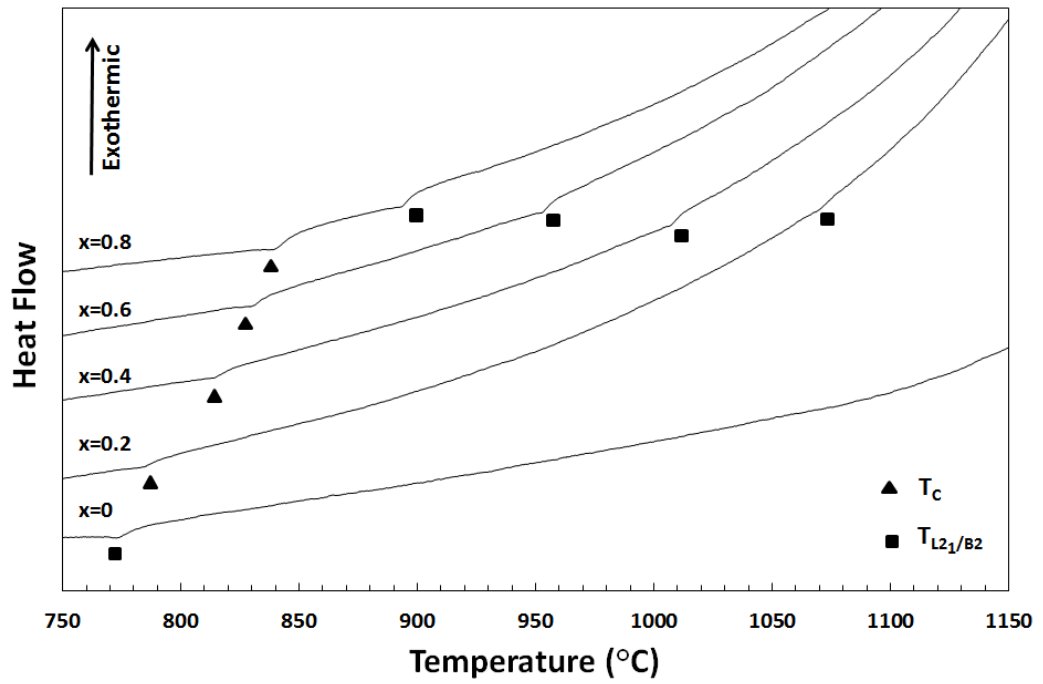


Figure 4.21 DSC patterns of $\text{Co}_2\text{FeSi}_{1-x}\text{Ga}_x$ ($x=0, 0.2, 0.4, 0.6, 0.8$ and 1) alloy system annealed at $(T_{L2_1/B2} - 100^\circ\text{C})$ for 5 days, obtained at a heating rate of $10^\circ\text{C}/\text{min}$

The dependence of the T_C and $T_{L2_1/B2}$ as a function of the Ga composition in $\text{Co}_2\text{FeSi}_{1-x}\text{Ga}_x$ ($x=0, 0.2, 0.4, 0.6, 0.8$ and 1) alloy system are displayed in Figure 4.22. A representative graph is plotted for $\text{Co}_2\text{FeSi}_{1-x}\text{Ga}_x$ ($x=0, 0.2, 0.4, 0.6, 0.8$ and 1) alloy annealed at 1027°C since there is not a serious effect of the annealing temperatures on the T_C and $T_{L2_1/B2}$. From graph, it is verified that the $T_{L2_1/B2}$ is reduced by increasing x . All the $T_{L2_1/B2}$ values form a linear line as reported in quaternary Co-based Heusler alloys [37-38]. This can be explained with Bragg-Williams-Gorksy (BWG) approximation [43-44]. They assumed that the variety in the order-disorder phase transition temperature, $T_{L2_1/B2}$ can be anticipated to be proportional to the concentration of the substitutional element Z' if X elements perfectly occupy ordered in X_2YZ Heusler alloy.

As shown in Figure 4.22, the T_C show an increment with increasing x , displaying an upward convexity. Similar behavior of T_C versus composition is seen in the $\text{Co}_2\text{Cr}_{1-x}\text{Fe}_x\text{Ga}$ [36], $\text{Co}_2\text{V}_{1-x}\text{Mn}_x\text{Ga}$ [38], $\text{Co}_2\text{Ti}_{1-x}\text{Mn}_x\text{Ga}$ [39] and $\text{Co}_2\text{MnGa}_{1-x}\text{Z}_x$ [45] alloys. Okubo and his co-workers reported that the composition dependences of the Curie temperature for the quaternary $\text{Co}_2\text{MnGa}_{1-x}\text{Z}_x$ alloys may be related with the mixture of the magnetic moment and the lattice parameters. They found that there is inverse proportion between the lattice parameter and the Curie temperature. However, in this study, the Curie temperature for $\text{Co}_2\text{FeSi}_{1-x}\text{Ga}_x$ increases with increasing of Ga composition except for $x=1$ while the lattice parameter increases, according to Vegard's law the lattice parameter increases with increasing Ga composition (see Appendix B). In order to understand the behavior of the T_C , more detailed investigations would be required.

In order to accomplish practical applications in spintronic devices, ferromagnetic materials with a high T_C at and above room room temperature is desired. Therefore,

the present quaternary alloy system, $\text{Co}_2\text{FeSi}_{1-x}\text{Ga}_x$ ($x=0, 0.2, 0.4, 0.6, 0.8$ and 1), can be favoured candidate because of high T_C value in between 773°C and 787°C .

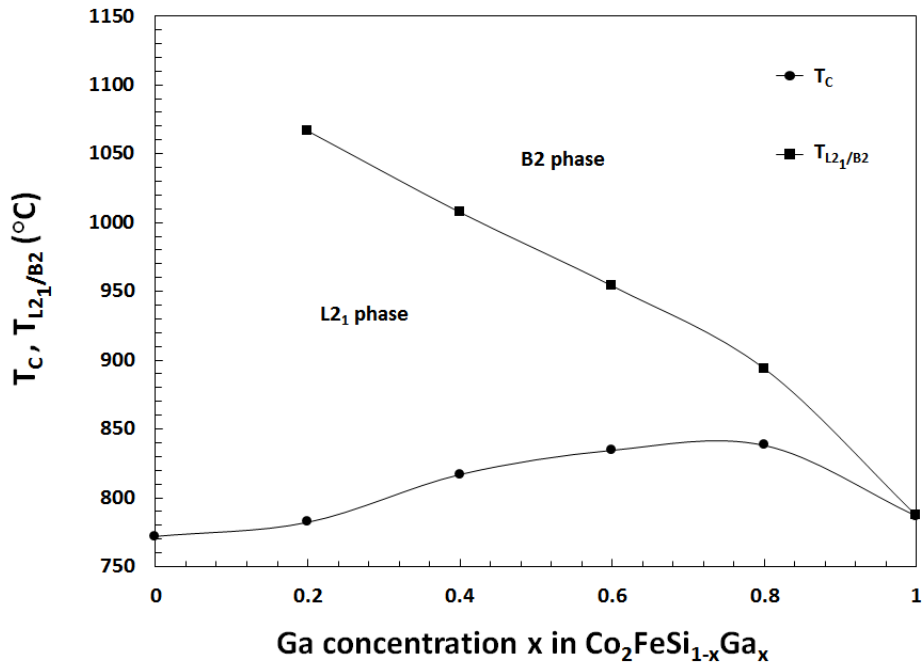


Figure 4.22 Composition dependence of T_C and $T_{L2_1/B2}$ $\text{Co}_2\text{FeSi}_{1-x}\text{Ga}_x$ ($x=0, 0.2, 0.4, 0.6, 0.8$ and 1) alloy system annealed at 1027°C for 20 days

4.2.3 Effects of heat treatment on the magnetic properties of the $\text{Co}_2\text{FeSi}_{1-x}\text{Ga}_x$ alloy system

In order to characterize the magnetic properties of the heat treated $\text{Co}_2\text{FeSi}_{1-x}\text{Ga}_x$ ($x=0, 0.2, 0.4, 0.6, 0.8$ and 1) alloy system, magnetic field dependence of magnetization is measured.

Figures 4.23-4.25 display the magnetization as a function of magnetic field for the $\text{Co}_2\text{FeSi}_{1-x}\text{Ga}_x$ ($x=0, 0.2, 0.4, 0.6, 0.8$ and 1) alloy system annealed at 1027°C for 20 days, ($T_{L2_1/B2}+40^\circ\text{C}$) for 5 days and ($T_{L2_1/B2}-100^\circ\text{C}$) for 5 days, respectively. Magnetization curves show ferromagnetic behaviour for all compositions and heat treatment temperatures. Moreover, it is noted that all samples are soft magnetic with a small remance. Increasing the Ga concentration decreases the saturation magnetization value. In table 4.7, the magnetic properties are given.

Table 4.7 Magnetic properties measured at RT for the as-cast and annealed $\text{Co}_2\text{FeSi}_{1-x}\text{Ga}_x$ ($x=0, 0.2, 0.4, 0.6, 0.8$ and 1) alloy system. Saturation magnetization and remanent magnetization are denoted by M_s (emu g^{-1}) and M_r (emu g^{-1}) respectively

ALLOY	As-cast			1027 °C			(T +40) °C			(T -100) °C		
	M_s	M_r	M_s	M_r	M_s	M_r	M_s	M_r	M_s	M_r	M_s	M_r
Co_2FeSi	125	0.187	178	0.468	165	0.111	136	0.531				
$\text{Co}_2\text{FeSi}_{0.8}\text{Ga}_{0.2}$	121	0.085	162	0.165	146	0.100	129	0.089				
$\text{Co}_2\text{FeSi}_{0.6}\text{Ga}_{0.4}$	118	0.114	153	0.054	142	0.035	131	0.024				
$\text{Co}_2\text{FeSi}_{0.4}\text{Ga}_{0.6}$	112	0.021	129	0.069	138	0.061	136	0.07				
$\text{Co}_2\text{FeSi}_{0.2}\text{Ga}_{0.8}$	102	0.025	115	0.011	128	0.022	130	0.032				
Co_2FeGa	78	0.035	97	0.025	100	-	108	-				

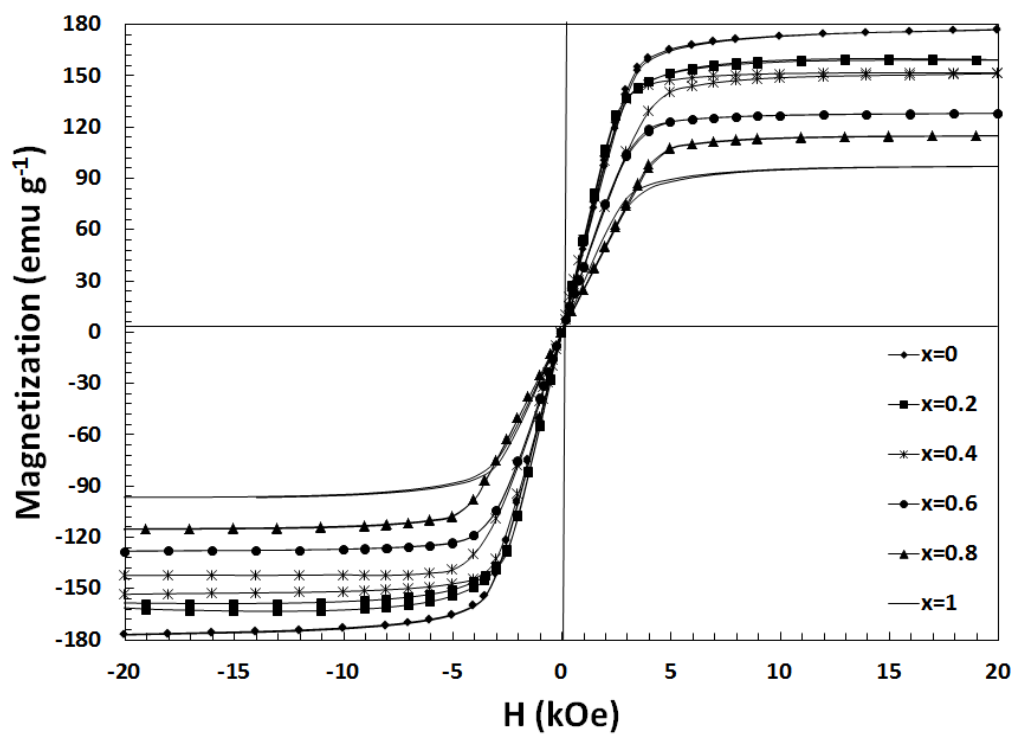


Figure 4.23 Magnetization of the $\text{Co}_2\text{FeSi}_{1-x}\text{Ga}_x$ ($x=0, 0.2, 0.4, 0.6, 0.8$ and 1) alloy system annealed at 1027°C for 20 days as a function of magnetic field measured at RT

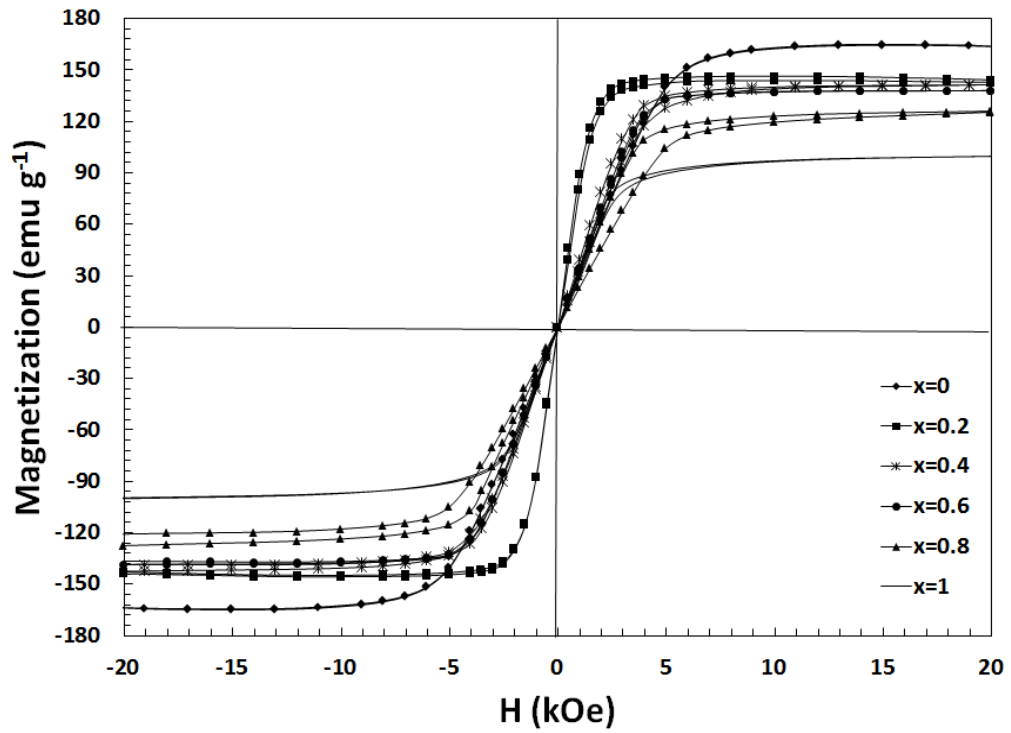


Figure 4.24 Magnetization of the $\text{Co}_2\text{FeSi}_{1-x}\text{Ga}_x$ ($x=0, 0.2, 0.4, 0.6, 0.8$ and 1) alloy system annealed at $(T_{L2_1/B2} + 40^\circ\text{C})$ for 5 days as a function of magnetic field measured at RT

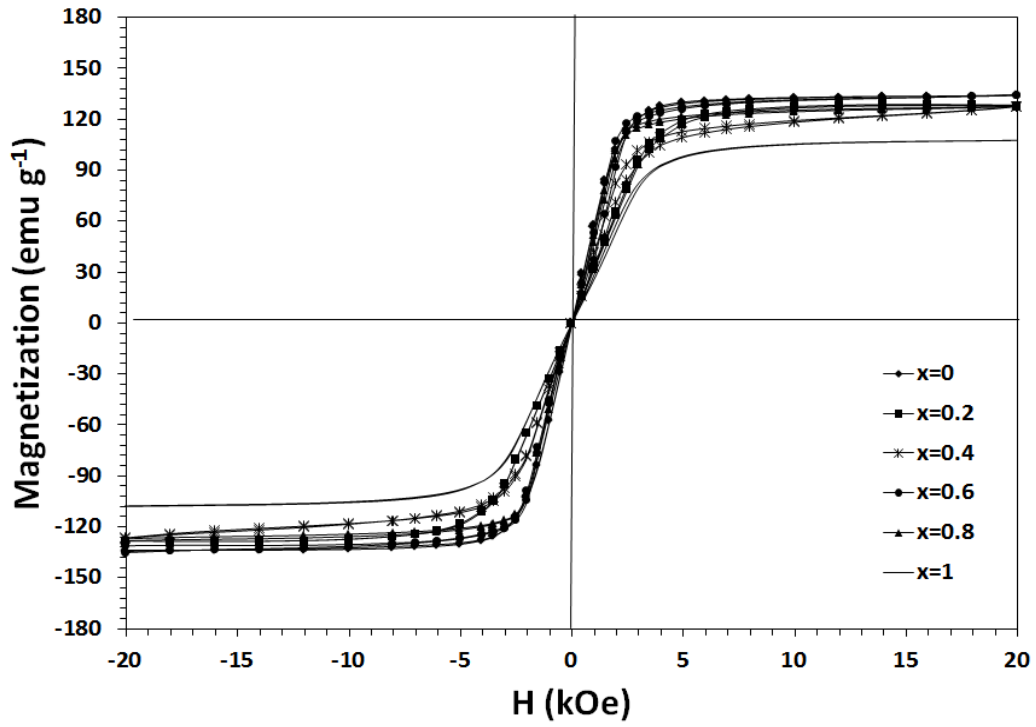


Figure 4.25 Magnetization of the $\text{Co}_2\text{FeSi}_{1-x}\text{Ga}_x$ ($x=0, 0.2, 0.4, 0.6, 0.8$ and 1) alloy system annealed at ($T_{L2_1/B2} - 100^\circ\text{C}$) for 5 days as a function of magnetic field measured at RT

Shown in Figure 4.26-4.31 demonstrate that the magnetic properties of the $\text{Co}_2\text{FeSi}_{1-x}\text{Ga}_x$ ($x=0, 0.2, 0.4, 0.6, 0.8$ and 1) alloy system is sensitive to the annealing temperature. It was reported that the magnetic properties of the $\text{Co}_2\text{Cr}_{1-x}\text{Fe}_x\text{Al}$ alloys changes with the degree of disorder. The magnetic moment of the $\text{Co}_2\text{Cr}_{1-x}\text{Fe}_x\text{Al}$ alloys reduce with decreasing the degree of long range order. In the present study, ferromagnetic properties are observed in the $\text{Co}_2\text{FeSi}_{1-x}\text{Ga}_x$ ($x=0, 0.2, 0.4, 0.6, 0.8$ and 1) alloy system. On the other hand, the saturatization magnetization of the L2_1 phase is not the same with the saturation magnetization of the B2 phase. The B2 -type disorder, which interchanges Fe with Si and Ga, conducts to a small decrease of the saturatization magnetization compared to the L2_1 ordered structure. On the contrary, the A2 -type disorder, which is randomly distribution of all atoms, conducts to a significant decrease in the saturation magnetization with increasing the degree of disorder. The effect of the atomic ordering on the magnetic properties for the $\text{Co}_2\text{FeSi}_{1-x}\text{Ga}_x$ alloys has not been made clear yet. In order to understand this situation, the theoritical calculations can be done on electrons of atoms occupying Co, Fe, Si and Ga sites.

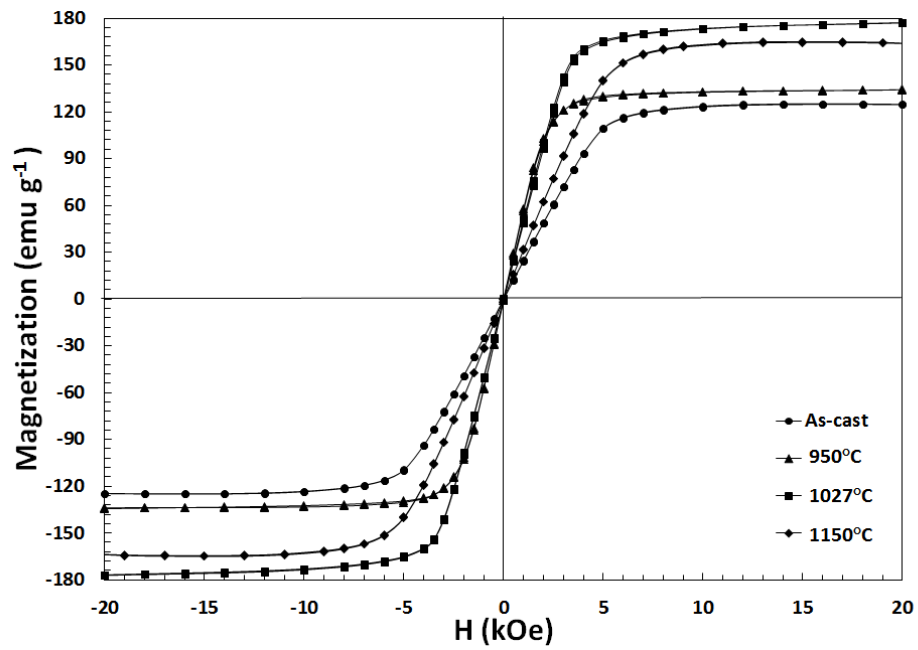


Figure 4.26 Magnetization curves of the Co_2FeSi alloy annealed at 950°C for 5 days, 1027°C for 20 days and 1150°C for 5 days as a function of magnetic field measured at RT

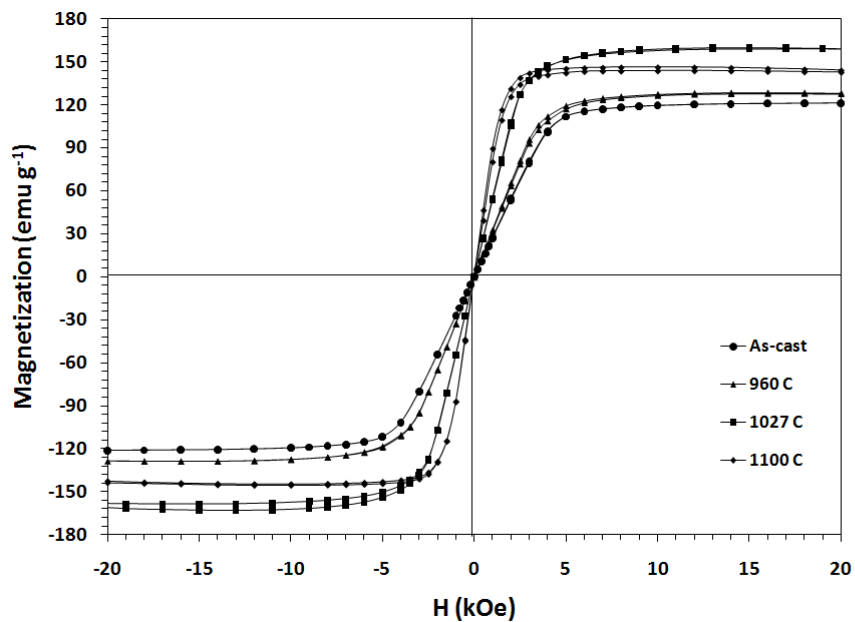


Figure 4.27 Magnetization curves of the $\text{Co}_2\text{FeSi}_{0.8}\text{Ga}_{0.2}$ alloy annealed at 960°C ($T_{L2_1/B2} - 100^\circ\text{C}$) for 5 days, 1027°C for 20 days and 1100°C ($T_{L2_1/B2} + 40^\circ\text{C}$) for 5 days as a function of magnetic field measured at RT

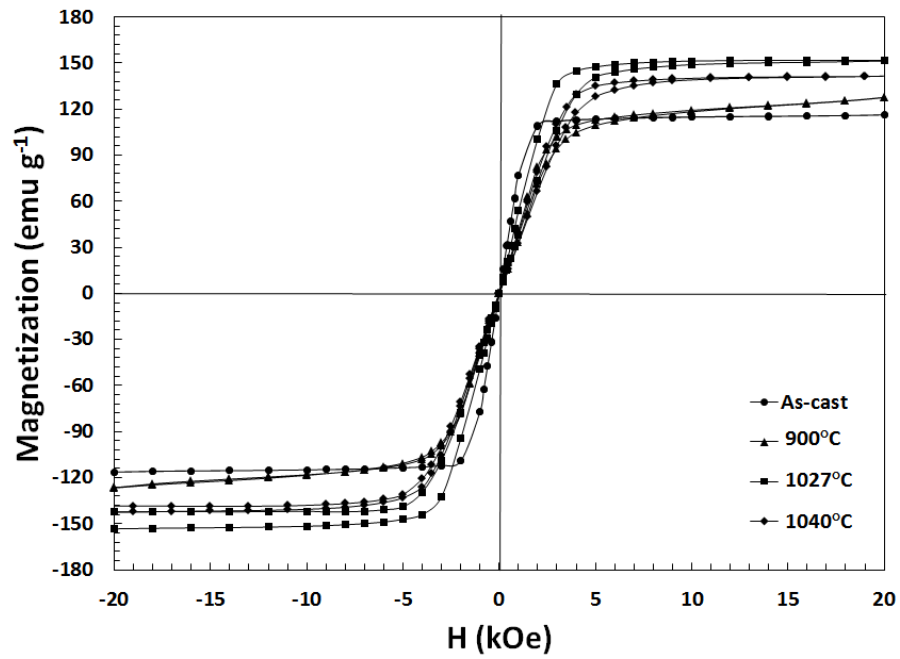


Figure 4.28 Magnetization curves of the $\text{Co}_2\text{FeSi}_{0.6}\text{Ga}_{0.4}$ alloy annealed at 900°C ($T_{L_{2_1/B_2}} - 100^\circ\text{C}$) for 5 days, 1027°C for 20 days and 1040°C ($T_{L_{2_1/B_2}} + 40^\circ\text{C}$) for 5 days as a function of magnetic field measured at RT

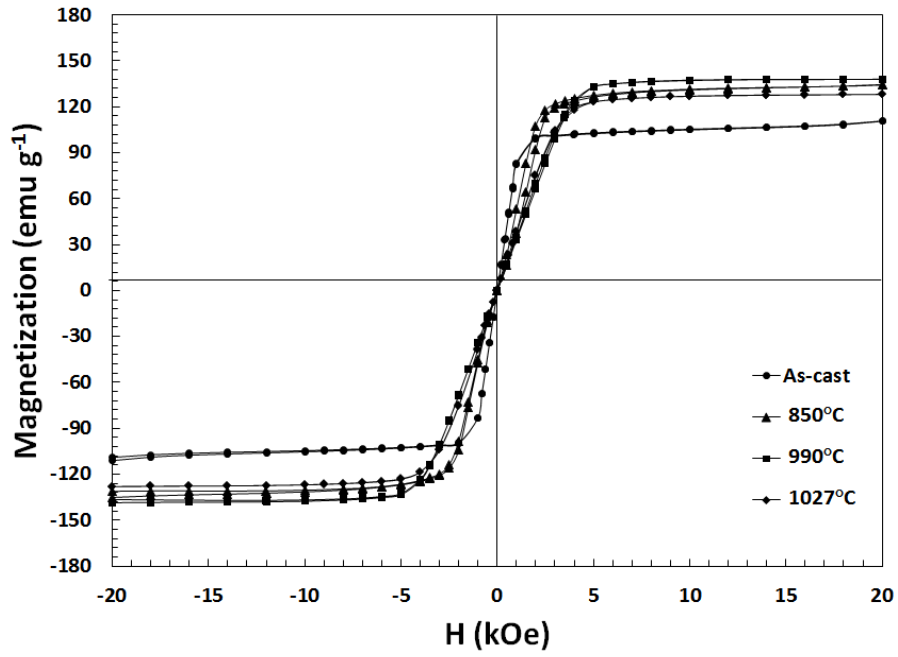


Figure 4.29 Magnetization curves of the $\text{Co}_2\text{FeSi}_{0.4}\text{Ga}_{0.6}$ alloy annealed at 850°C ($T_{L_{21}/B_2} - 100^\circ\text{C}$) for 5 days, 990°C ($T_{L_{21}/B_2} + 40^\circ\text{C}$) for 5 days, and 1027°C for 20 days as a function of magnetic field measured at RT

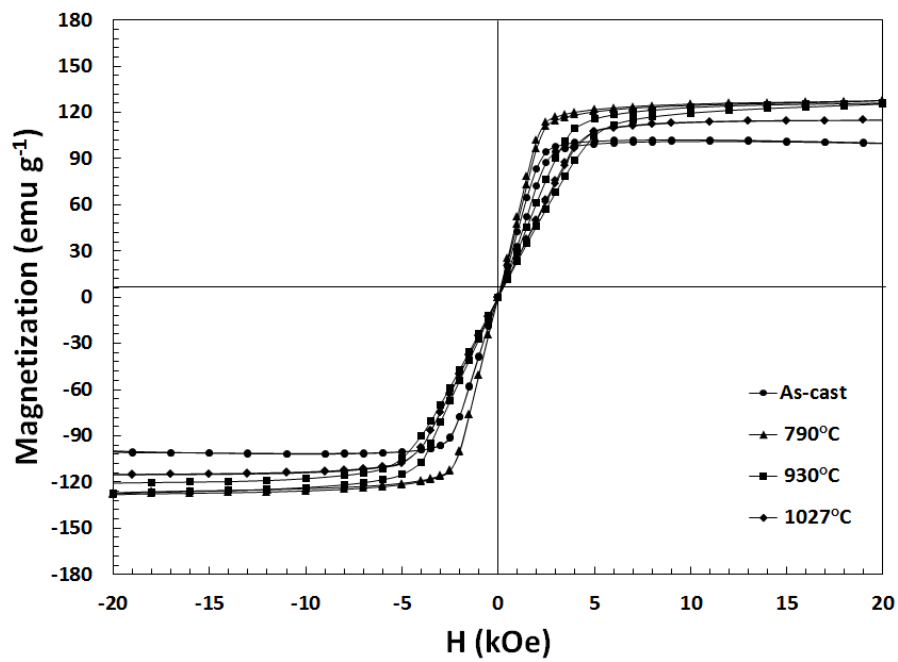


Figure 4.30 Magnetization curves of the $\text{Co}_2\text{FeSi}_{0.2}\text{Ga}_{0.8}$ alloy annealed at 790°C ($T_{L2_1/B2} - 100^\circ\text{C}$) for 5 days, 930°C ($T_{L2_1/B2} + 40^\circ\text{C}$) for 5 days, and 1027°C for 20 days as a function of magnetic field measured at RT

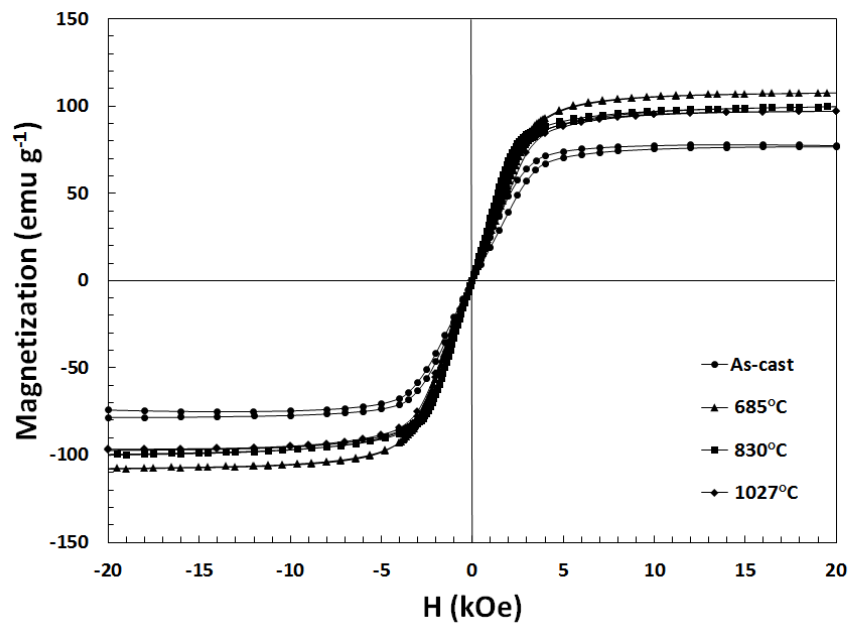


Figure 4.31 Magnetization curves of the Co₂FeGa alloy annealed at 685°C ($T_{L_{2_1}/B_2} - 100^\circ\text{C}$) for 5 days, 830°C ($T_{L_{2_1}/B_2} + 40^\circ\text{C}$) for 5 days as a function of magnetic field measured at RT

CHAPTER 5

CONCLUSIONS

The main aim of the present study is to determine the composition and the heat treatment dependence on the phase stability of $L2_1$ phase for the $Co_2FeSi_{1-x}Ga_x$ alloys. The substitutional series of the quaternary Heusler alloys $Co_2FeSi_{1-x}Ga_x$ were produced by arc melting and their structural and magnetic properties have been investigated experimentally. During the solidification and heat treatment, the Heusler alloys undergo a series of transformation: structural ($L2_1 \leftrightarrow B2$) and magnetic (ferromagnetic \leftrightarrow paramagnetic). The results are important to understand the relationship between the structure and magnetic properties in Heusler alloys. The obtained results are concluded as following:

- Enhance of the magnetic properties strongly depends on the $L2_1$ phase formation. Various heat treatment processes revealed that there is significant sensitivity to annealing temperature and time to provide the $L2_1$ structure. For high Si concentration, high annealing temperature and long period are required. However, the annealing temperature and time decrease with increasing Ga concentration.
- The values of the $L2_1$ -B2 order-order structural transition temperature and the Curie temperature approach each other with increasing Ga composition; on the other hand, these temperatures are almost the same with varying the annealing temperature.

- While the L₂₁-B2 order-order structural transition temperature reduces, the Curie temperature enhances with enhancing Ga content.
- Magnetic properties improve with heat treatment. The saturation magnetization of the L₂₁ structure is higher than the B2 structure since the magnetic properties are related with the degree of long range order. However, it decreases with increasing Ga content.
- Among the alloys studied, the Co₂FeSi_{0.2}Ga_{0.8} Heusler alloy heat treated below the L₂₁-B2 order-order transition temperature crystallized in the ordered L₂₁ structure and it has the highest Curie temperature (834°C) within the Co₂FeSi_{1-x}Ga_x alloys. Therefore, the Co₂FeSi_{0.2}Ga_{0.8} alloy may be chosen as optimum composition for spintronics applications.

REFERENCES

1. A. J. Bradley, J. W. Rodgers, *Proceedings of Royal Society A*, 1934. **144**: p. 340.
2. F. Heusler, *Verh. Dtsch. Phys. Ges*, 1903. **5**: p. 219
3. H. Potter, *Proceedings of the Physical Society*, 1928. **41/1**: p. 135.
4. J. Kübler, A. William, C. Sommers, *Phys Rev B*, 1983. **28/4**: p. 1745.
5. C. Felser, G. H. Fecher, B. Balke, *Angewandte Chemie (International ed. in English)*, 2007. **46/5**: p. 668.
6. D. Jung, *J Mol Struct: Theochem*, 2000. **527/1-3**: p. 113.
7. J. H. Wernick, G. W. Hull, T. H. Geballe, J. E. Bernardini, J. V. Waszczak, *Mater Lett*, **2/2**: p. 90.
8. R. Y. Umetsu, K. Kobayashi, a Fujita, R. Kainuma, K. Ishida, *J Appl Phys*, 2008. **103/7**: p. 07D718.
9. M. Kogachi, T. Fujiwar, S. Kikuchi, *J. Alloys Compd.*, 2009. **475/1-2**: p. 723.
10. S. Wurmehl, G. Fecher, H. Kandpal, *Appl phys*, 2006. **99**: p. 1.
11. M. Zhang, E. Brück, F. R. de Boer, Z. Li, W. Guangheng, *J. Phys. D: Appl. Phys.*, 2004. **37**: p. 2049.
12. G. Prathiba, S. Venkatesh, M. Rajagopalan, N. Harish Kumar, *J Magn Magn Mater*, 2011. **323/1**: p. 22.

13. G. H. Fecher, H. C. Kandpal, S. Wurmehl, J. Morais, H. J. Lin, H. J. Elmers, G. Schönhense, C. Felser, *J Phys: Condensed Matter*, 2005. **17/46**: p. 7237.
14. S. Wurmehl, G. H. Fecher, H. C. Kandpal, V. Ksenofontov, C. Felser, H. J. Lin, J. Morais, *Phys Rev B*, 2005. **72/18**: p. 184434.
15. S. Wurmehl, G. H. Fecher, V. Ksenofontov, F. Casper, U. Stumm, C. Felser, H. J. Lin, Y. Hwu, *J Appl Phys*, 2006. **99/8**: p. 08J103.
16. T. Graf, C. Felser, S. S. P. Parkin, *Prog Solid State Ch*, 2011. **39/1**: p. 1.
17. Y. Miura, K. Nagao, M. Shirai, *Phys Rev B*, 2004. **69/14**: p. 1.
18. H. C. Kandpal, V. Ksenofontov, M. Wojcik, R. Seshadri, C. Felser, *J Phys D: Appl Phys*, 2007. **40/6**: p. 1587.
19. S. Picozzi, A. Continenza, A. J. Freeman, *Phys Rev B*, 2004. **69**: p. 094423.
20. G. E. Bacon, J. S. Plant, *J Phys F: Metal Physics*, 1971. **1/4**: p. 524.
21. T. Graf, F. Casper, J. Winterlik, B. Balke, G. H. Fecher, C. Felser, *Zeitschrift für anorganische und allgemeine Chemie*, 2009. **635/6-7**: p. 976.
22. Y. Kota, A. Sakuma, *J Phys: Conference Series*, 2011. **266**: p. 012094.
23. M. Jin, J. Liu, X. Jin, *Intermetallics*, 2010. **18/5**: p. 846.
24. B. Ravel, J. O. Cross, M. P. Raphael, V. G. Harris, R. Ramesh, V. Saraf, *Appl Phys Lett*, 2002. **81/15**: p. 2812.
25. R. Y. Umetsu, K. Kobayashi, R. Kainuma, Y. Yamaguchi, K. Ohoyama, A. Sakuma, K. Ishida, *J Alloy Compd*, 2010. **499/1**: p. 1.
26. P. J. Webster, K. R. A. Ziebeck, *Landolt-Börnstein, New Series, Group III*. Berlin: 1988. p. 75.

27. R. A. de Groot, F. M. Mulleer, P. G. Van Engen, K. H. J. Buschow, *Phys Rev Lett*, 1983. **50/25**: p. 2024.
28. J. C. Slater, *Phys. Rev.*, 1930. **36**: p. 57.
29. L. Pauling, *Phys Rev*, 1938. **54/11**: p. 899.
30. B. S. D. Ch. S. Varaprasad, A. Rajanikanth, Y. K. Takahashi, K. Hono, *Acta Mater*, 2009. **57/9**: p. 2702.
31. M. Kogachi, N. Tadachi, T. Nakanishi, *Intermetallics*, 2006. **14/7**: p. 742.
32. A. Okubo, R. Y. Umetsu, M. Nagasako, A. Fujita, R. Kainuma, K. Ishida, *Scripta Mater*, 2008. **59/8**: p. 830.
33. K. Kobayashi, R.Y. Umetsu, A. Fujita, K. Oikawa, R. Kainuma, K. Fukamichi, K. Ishid, *J Alloy Compd*, 2005. **399/1-2**: p. 60.
34. C. Topbaşı, “Theoretical and Experimental Investigations on Atomic and Magnetic Ordering in Full Heusler Alloys,” Middled East Technical University, 2008.
35. G. H. Fecher, H. C. Kandpal, S. Wurmehl, C. Felser, G. Schönhense, *J Appl Phys*, 2006. **99/8**: p. 08J106.
36. R. Umetsu, K. Kobayashi, A. Fujita, K. Oikawa, R. Kainuma, K. Ishid, *Phys Rev B*, 2005. **72**: p. 214412
37. R. Y. Umetsu, K. Kobayashi, A. Fujita, R. Kainuma, K. Ishida, *Scripta Mater*, 2008. **58/9**: p. 723.
38. R. Umetsu, K. Kobayashi, A. Fujita, R. Kainuma, K. Ishida, K. Fukamichi, A. Sakuma, *Phys Rev B*, 2008. **77/10**: p. 1.
39. A. Okubo, R. Y. Umetsu, R. Kainuma, K. Ishida, *J Phys: Conference Series*, 2010. **200**.

40. C. Felser, H. Elmers, G. H. Fecher, *Chem Inform*, 2006. **22**, p. 131.
41. H. Ishikawa, R.Y. Umetsu, K. Kobayashi, A. Fujita, R. Kainuma, K. Ishida, *Acta Mater*, 2008. **56**, p. 4789.
42. B. Balke, G. H. Fecher, H. C. Kandpal, C. Felser, *Phys. Rev. B*, 2006. **74**, p. 104405.
43. V. S. Gorsky, *Z. Phys.*, 1928, **50**, p. 64.
44. W. L. Bragg, E. J. Williams, *Proc. R. Soc. London, Ser. A* 145, 699 (1934); 151, 540 (1935)
45. A. Okubo, R. Y. Umetsu, K. Kobayashi, R. Kainuma, K. Ishida, *Appl Phys Lett*, 2010. **96**, p. 222507

APPENDIX A

EDX ANALYSES OF $\text{Co}_2\text{FeSi}_{1-x}\text{Ga}_x$ ALLOY SYSTEM

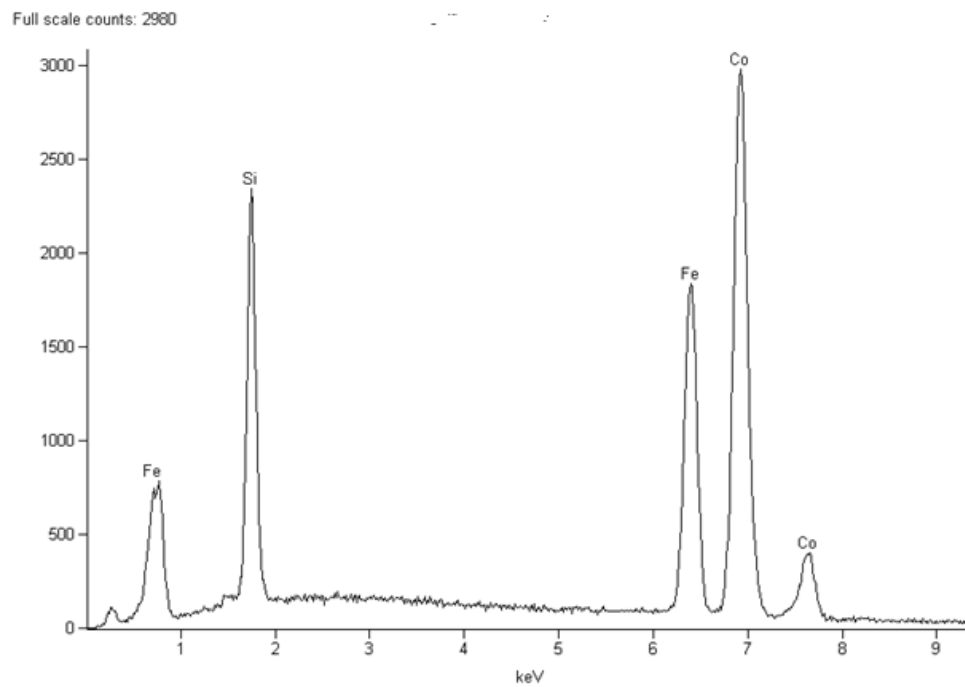


Figure A.1 EDX spectrum for the as-cast Co_2FeSi alloy

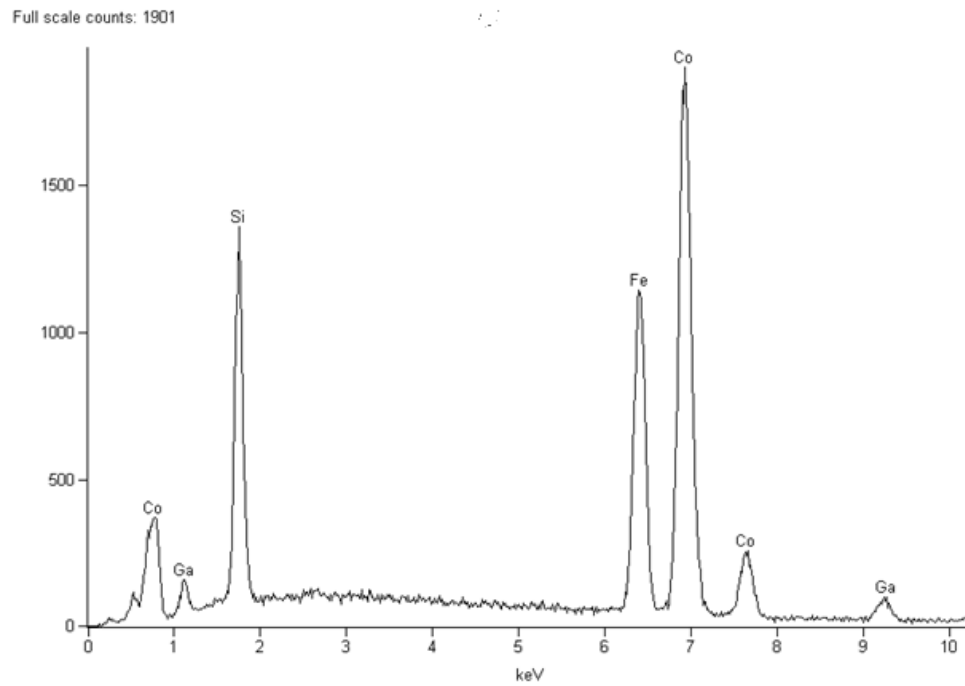


Figure A.2 EDX spectrum for the as-cast $\text{Co}_2\text{FeSi}_{0.8}\text{Ga}_{0.2}$ alloy

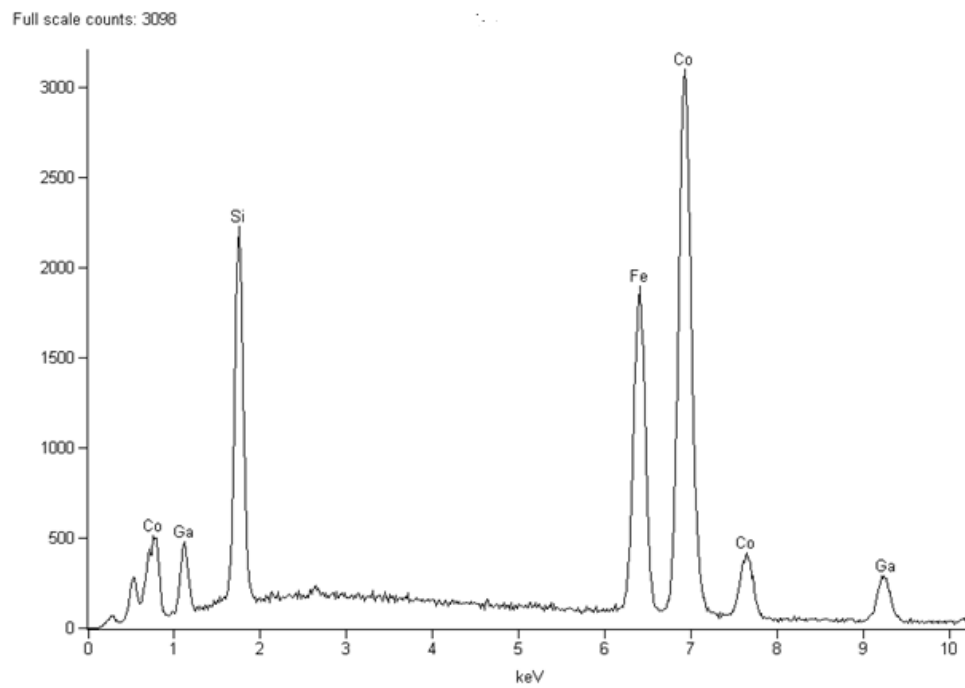


Figure A.3 EDX spectrum for the as-cast $\text{Co}_2\text{FeSi}_{0.6}\text{Ga}_{0.4}$ alloy

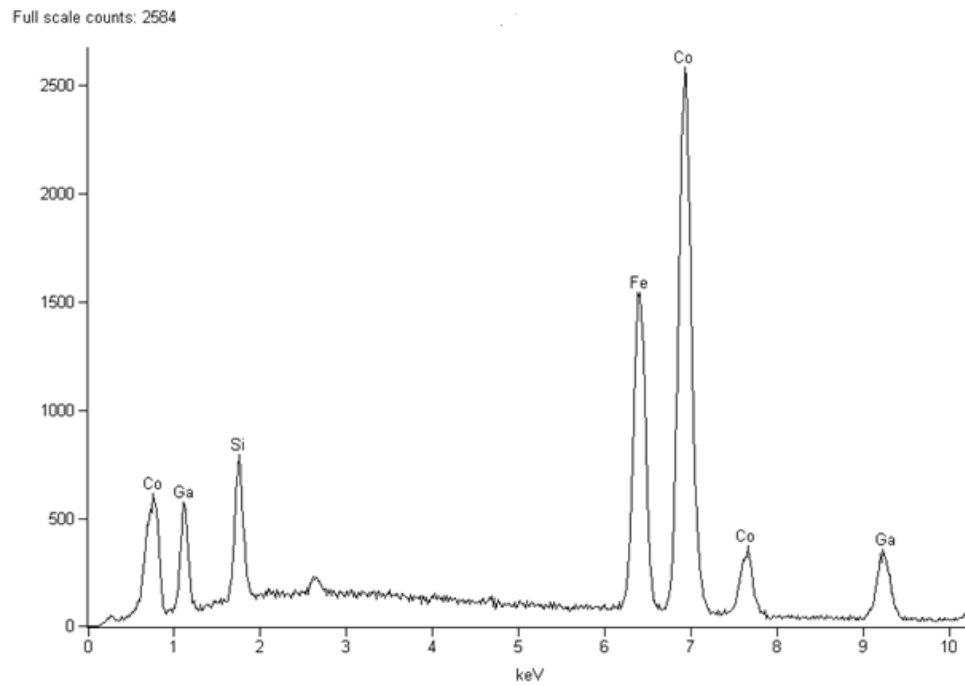


Figure A.4 EDX spectrum for the as-cast $\text{Co}_2\text{FeSi}_{0.4}\text{Ga}_{0.6}$ alloy

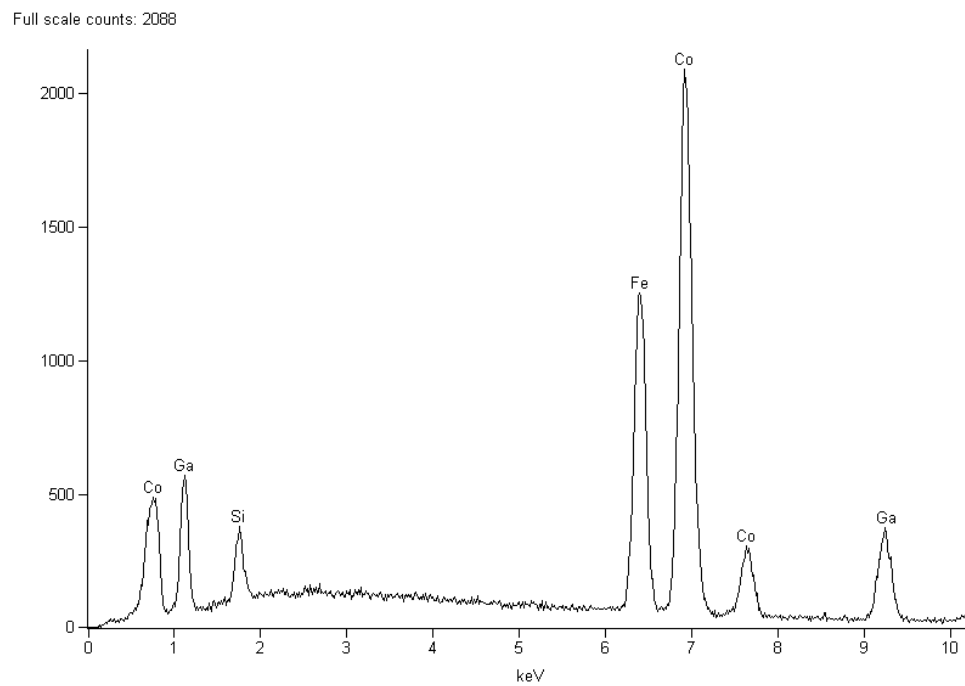


Figure A.5 EDX spectrum for the as-cast $\text{Co}_2\text{FeSi}_{0.2}\text{Ga}_{0.8}$ alloy

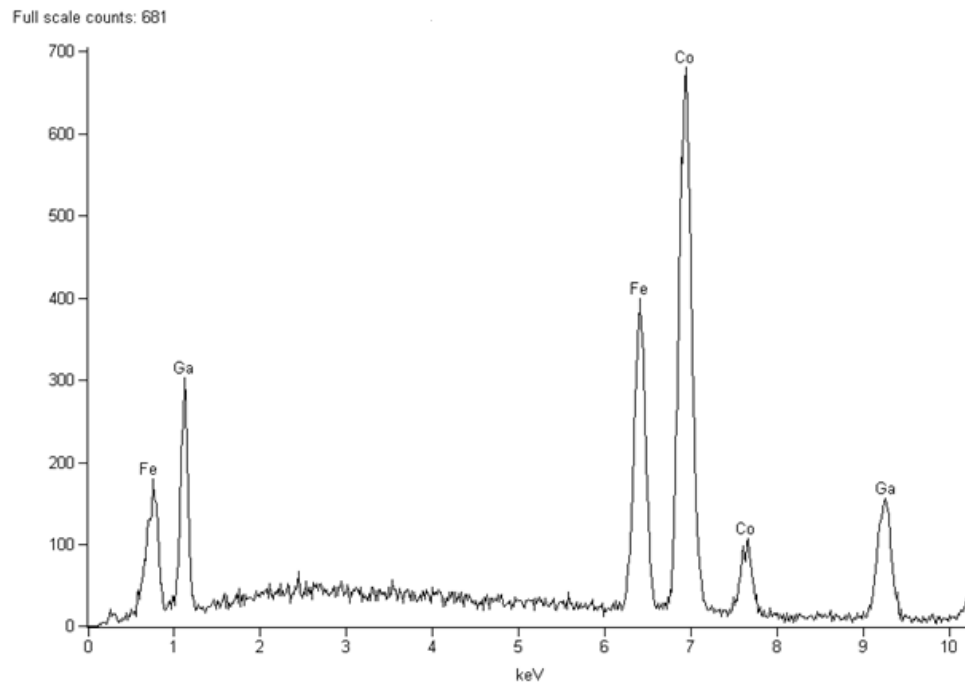


Figure A.6 EDX spectrum for the as-cast Co_2FeGa alloy

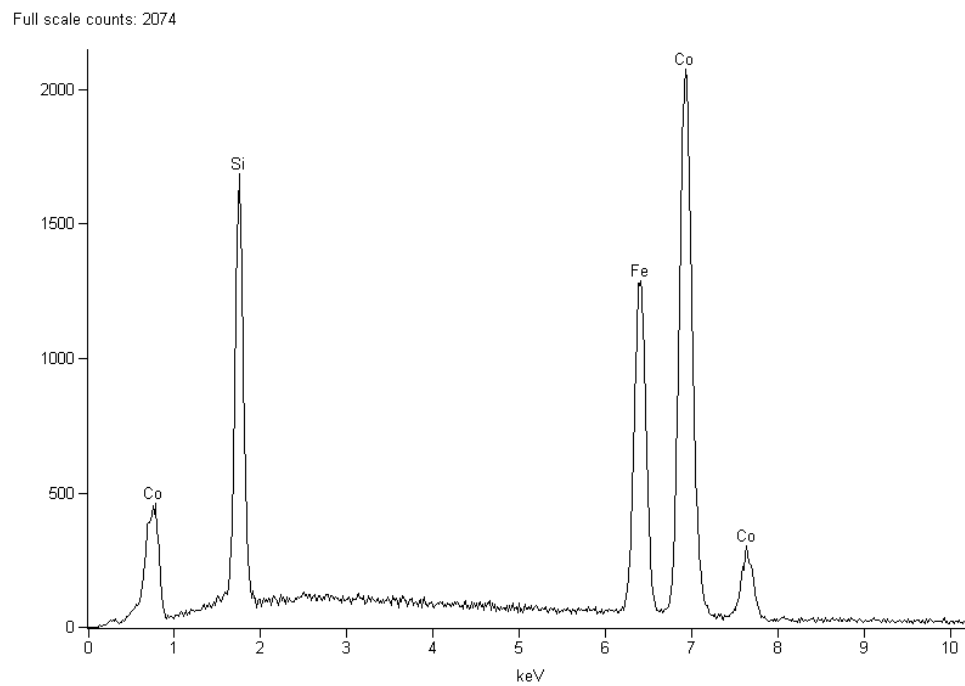


Figure A.7 EDX spectrum of the annealed Co_2FeSi alloy

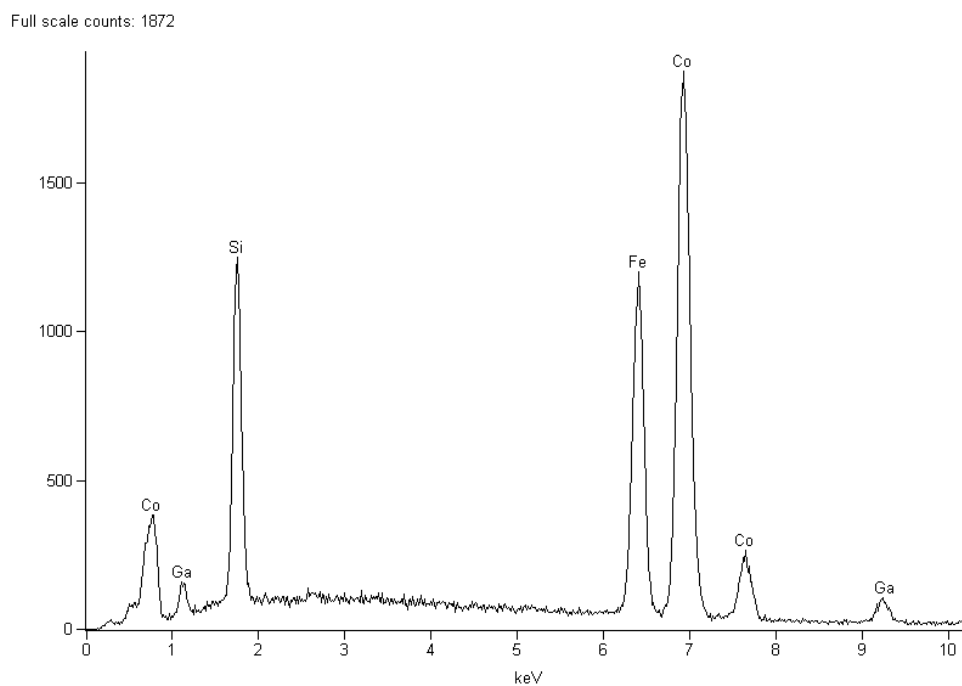


Figure A.8 EDX spectrum of the annealed $\text{Co}_2\text{FeSi}_{0.8}\text{Ga}_{0.2}$ alloy

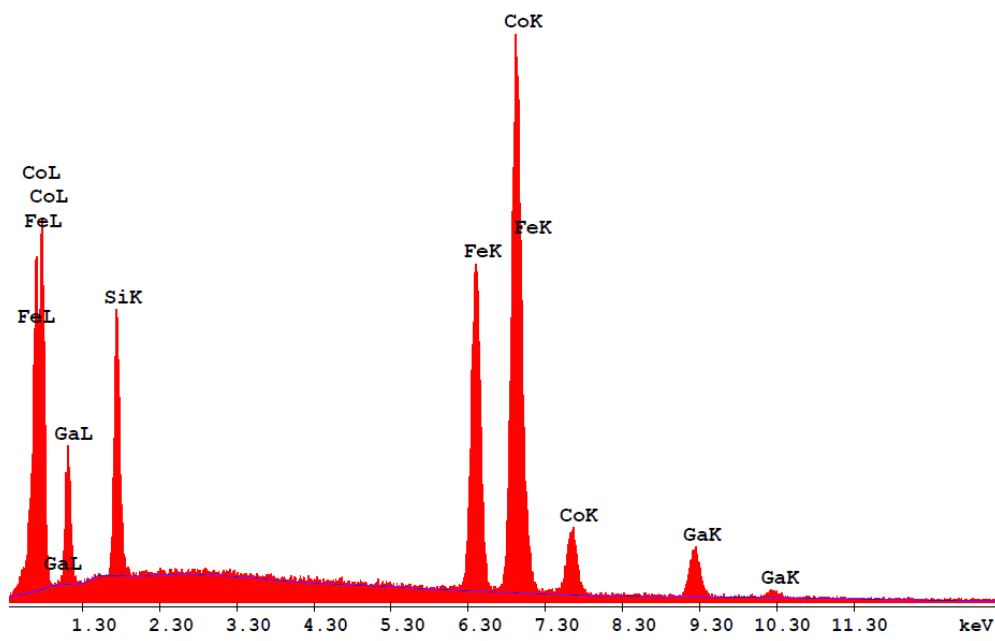


Figure A.9 EDX spectrum of the annealed $\text{Co}_2\text{FeSi}_{0.6}\text{Ga}_{0.4}$ alloy

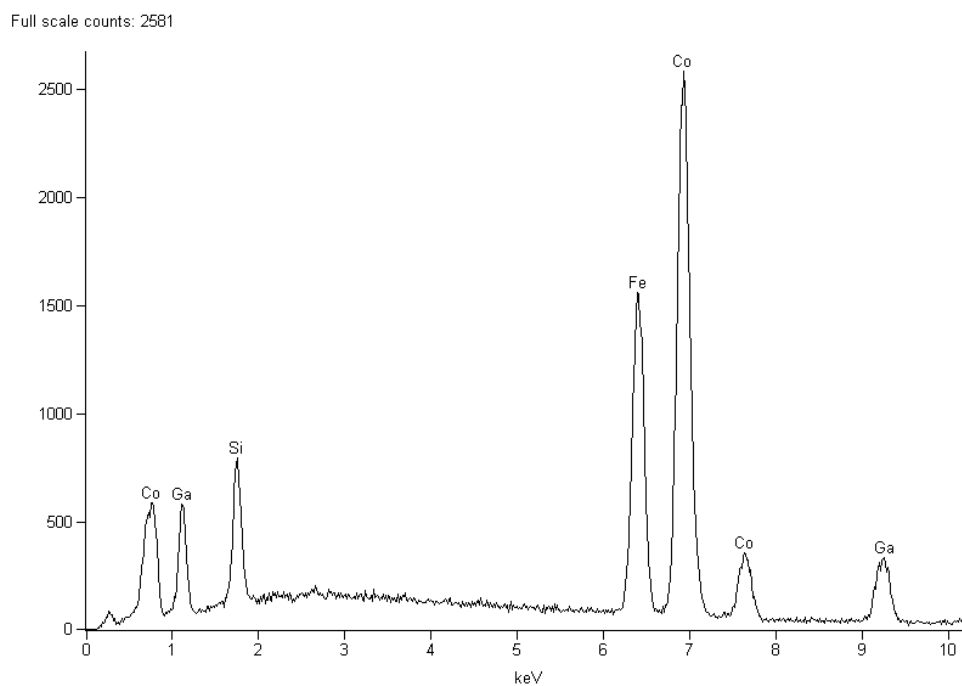


Figure A.10 EDX spectrum of the annealed $\text{Co}_2\text{FeSi}_{0.8}\text{Ga}_{0.6}$ alloy.

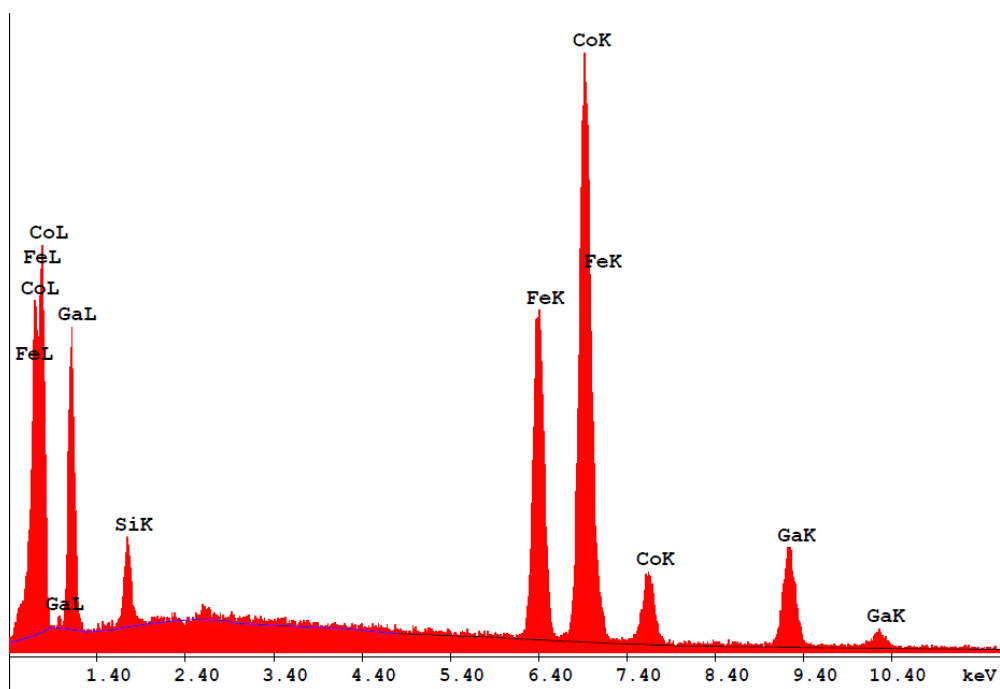


Figure A.11 EDX spectrum of the annealed $\text{Co}_2\text{FeSi}_{0.2}\text{Ga}_{0.8}$ alloy

Full scale counts: 1139

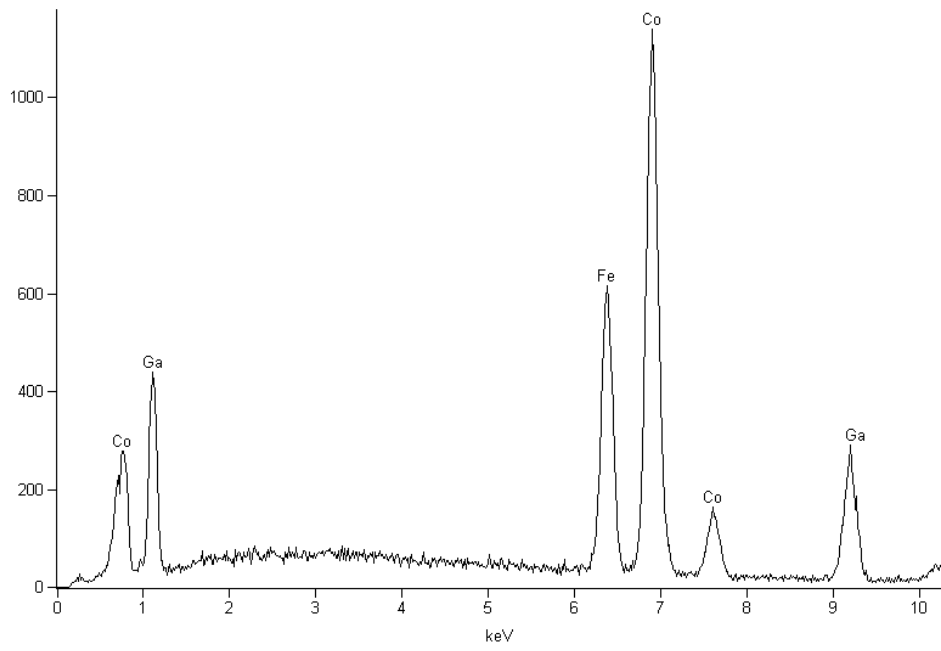


Figure A.12 EDX spectrum of the annealed Co_2FeGa alloy

APPENDIX B

VEGARD' S LAW

The calculated lattice parameter for the $\text{Co}_2\text{FeSi}_{1-x}\text{Ga}_x$ alloy system is computed by using following equation.

$$a = \%x_{\text{Si}}a_{\text{Co}_2\text{FeSi}} + \%x_{\text{Ga}}a_{\text{Co}_2\text{FeGa}}$$

Alloy	a (Å)
Co_2FeSi	5.64
$\text{Co}_2\text{FeSi}_{0.8}\text{Ga}_{0.2}$	5.66
$\text{Co}_2\text{FeSi}_{0.6}\text{Ga}_{0.4}$	5.68
$\text{Co}_2\text{FeSi}_{0.4}\text{Ga}_{0.6}$	5.70
$\text{Co}_2\text{FeSi}_{0.2}\text{Ga}_{0.8}$	5.72
Co_2FeGa	5.74

APPENDIX C

THERMAL ANALYSES OF $\text{Co}_2\text{FeSi}_{1-x}\text{Ga}_x$ ALLOY SYSTEM

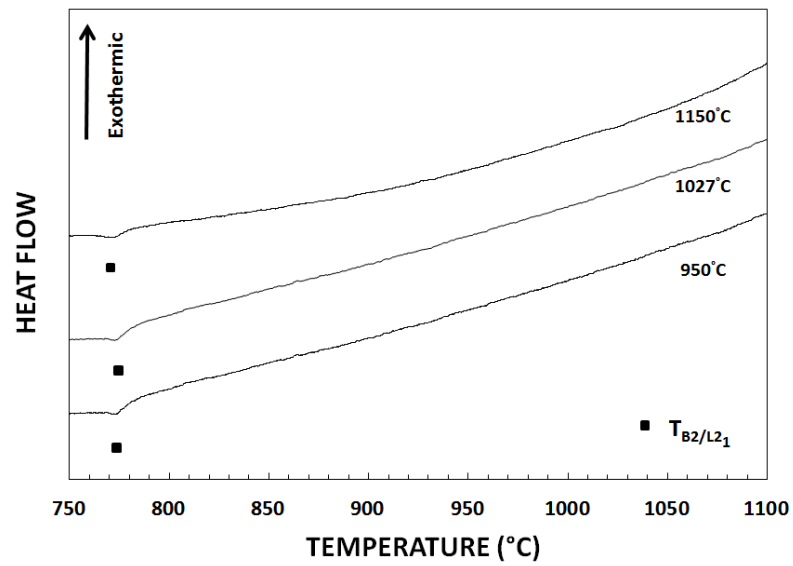


Figure C.1 DSC measurement for the Co_2FeSi alloy

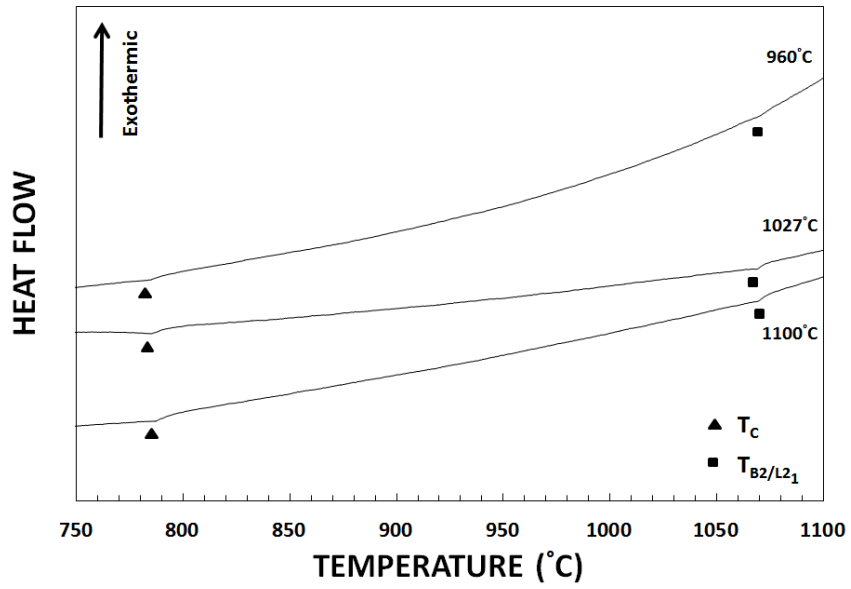


Figure C.2 DSC measurement for the $\text{Co}_2\text{FeSi}_{0.8}\text{Ga}_{0.2}$ alloy

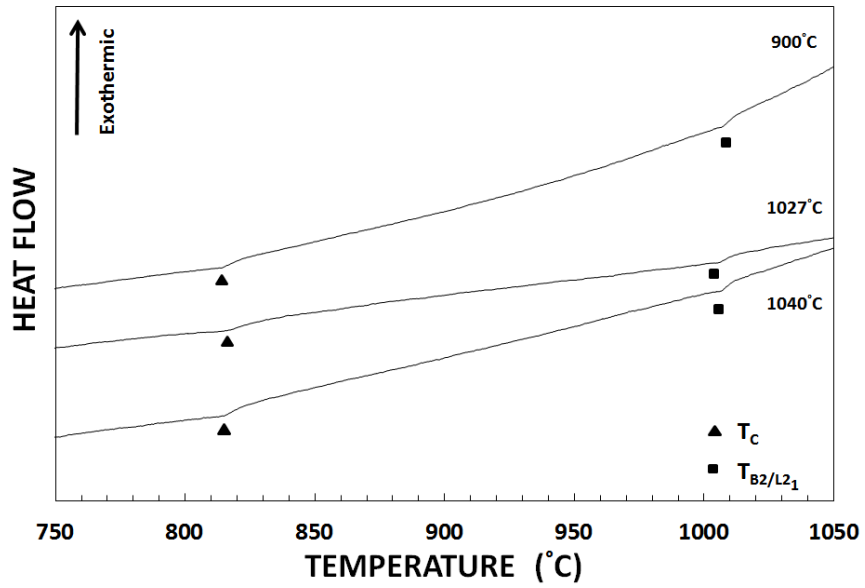


Figure C.3 DSC measurement for the $\text{Co}_2\text{FeSi}_{0.6}\text{Ga}_{0.4}$ alloy

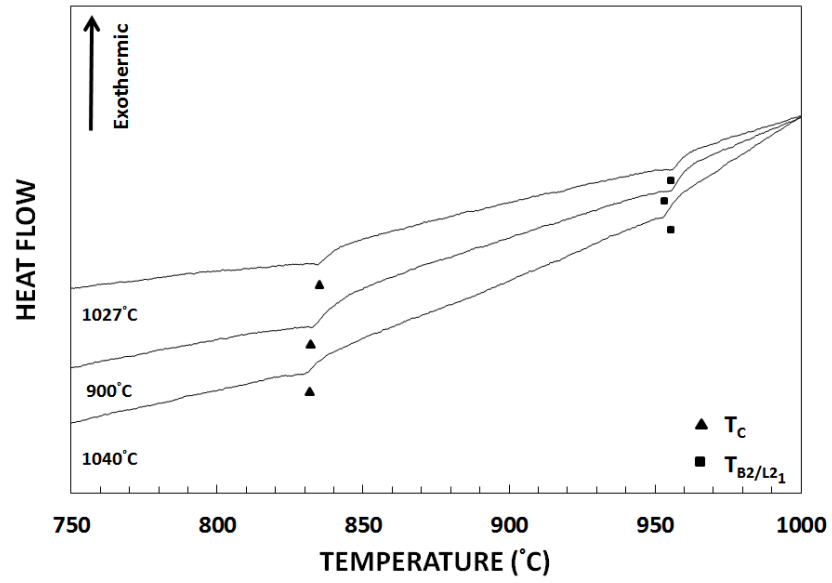


Figure C.4 DSC measurement for the $\text{Co}_2\text{FeSi}_{0.4}\text{Ga}_{0.6}$ alloy

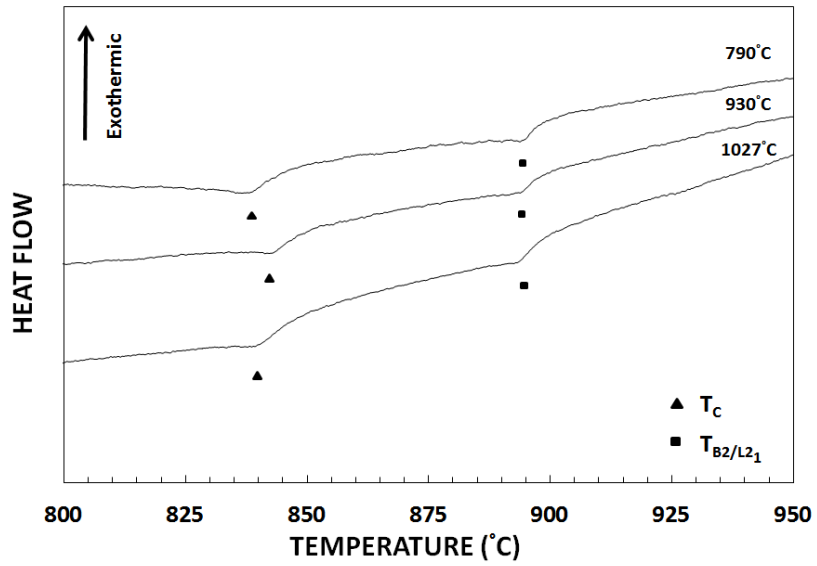


Figure C.5 DSC measurement for the $\text{Co}_2\text{FeSi}_{0.2}\text{Ga}_{0.8}$ alloy